Diploma Thesis

Acetic Acid Bioproduction by *Acetobacterium woodii* in Formate Medium in Continuous Bioreactors

Submitted in satisfaction of the requirements for the degree of
Diplom-Ingenieur
of the TU Wien, Faculty of Technical Chemistry

Diplomarbeit

Bioproduktion von Essigsäure durch *Acetobacterium woodii* in Formiat-Medium in kontinuierlichen Bioreaktoren

ausgeführt zum Zwecke der Erlangung des akademischen Grads
Diplom-Ingenieur
eingereicht an der TU Wien, Fakultät für Technische Chemie

von

Paul Zwerger

Matr.Nr.: 01607421

Betreuung: Assistant Prof. Dipl.-Ing.(FH) Dr. **Stefan Pflügl**

Institut für Verfahrenstechnik, Umwelttechnik und technische Biowissenschaften
Forschungsbereich der Bioverfahrenstechnik
Technische Universität Wien,
Getreidemarkt 9, 1060 Wien, Österreich

Wien, im November 2023

Abstract

Acetogens hold significant potential for sustainable chemical production, thanks to their autotrophic metabolism and the associated synthesis of CO_2 and H_2. This thesis focuses on *Acetobacterium woodii*, a microorganism capable of utilizing the Wood-Ljungdahl pathway, enabling it to assimilate formate. Formate can be generated from CO_2 using excess green energy and offers the advantage of easy transport in liquid or powder form.

The primary goal of this research is to perform continuous fermentation in a chemically defined medium with formate as the sole carbon and energy source while investigating the limits of formate feed concentration and dilution rate. Initially, experiments were conducted in serum bottles, followed by the evaluation of production and uptake rates and acetate yield during continuous fermentation.

The optimized strain achieved a dilution rate of 0.2 h^{-1}, resulting in a substantial volumetric acetate production rate of 12.6 mmol L^{-1} h^{-1} and an optimum acetate yield of 0.223 mol mol^{-1} at a dilution rate of 0.1 h^{-1}.

This work successfully demonstrated that *A. woodii* can efficiently metabolize formate to acetate in a chemically defined medium. The relatively high dilution rate of 0.2 h^{-1} is likely attributed to the biofilm formed on the reactor wall. From a production standpoint, a controlled biofilm as a cell retention system is advantageous and desired. To evaluate maximum growth rates and specific rates, measures must be taken to prevent biofilm formation. In summary, A. woodii represents a promising pathway for efficient and sustainable biosynthesis of bulk chemicals.

Keywords:

acetogen, *Acetobacterium woodii*, continuous bioreactor, sustainable acetic acid bioproduction, adaptive laboratory evolution, microorganism, Wood-Ljungdahl pathway, formate, carbon monoxide, bioprocess engineering

Table of contents

Table of figures

List of Abbreviations

ACS	=	Acetyl-CoA Synthase
ADP	=	Adenosine Diphosphate
ALE	=	Adaptive Laboratory Evolution
ATP	=	Adenosine Triphosphate
B_2	=	Riboflavin (Vitamin B2)
B_3	=	Nicotinic Acid (Vitamin B3)
B_5	=	Pantothenic Acid
CDM	=	Chemical Defined Medium
CODH	=	Carbon Monoxide Dehydrogenase
DoR	=	Degree of Reduction
Fd	=	Ferredoxin
Fd^{2-}	=	Reduced Ferredoxin
FAD	=	Flavin Adenine Dinucleotide
GC	=	Gas Chromatography
HDCR	=	Hydrogen-Dependent CO2 Reductase
HPLC	=	High-Performance Liquid Chromatography
mM	=	Millimolar (concentration unit)
N	=	Sample Size
NAD	=	Nicotinamide Adenine Dinucleotide
NADH	=	Reduced Nicotinamide Adenine Dinucleotide
NADP	=	Nicotinamide Adenine Dinucleotide Phosphate
OD_{600}	=	Optical Density at 600 nm
SEM	=	Standard Error of the Mean
SD	=	Standard Deviation
WLP	=	Wood-Ljungdahl Pathway
CDM	=	Chemical defined medium
YE	=	Yeast Extract

1 Introduction

1.1 General Background

The world faces the challenge of satisfying the energy needs required to sustain our modern standard of living due to the rapidly expanding global population. Presently, our global economy heavily depends on hydrocarbons, which were formed over millions of years. However, the unsustainable consumption of these finite resources contributes to the release of greenhouse gas emissions, which further leads to climate change (Khan et al., 2021). In response to the imperative challenges at hand, a methodical transformation of the linear energy and production economy towards a circular economy becomes essential (Patwa et al., 2021). Central to this aim is the integration of diverse solutions, including the implementation of renewable energy systems, the reduce, reuse, and recycle of consumer goods, the reengineering of processes for the conversion of both industrial and private waste streams, and the innovative direct utilization of carbon dioxide as a primary feedstock. These measures, though a fragment of conceivable solutions, exemplify the strategies that hold promise in circumventing the current challenges (Velenturf & Purnell, 2021).

While no single technology can fully meet our current energy needs and consumption demands, a comprehensive approach combined with energy-saving practices and improved efficiency technologies can lead us towards a more sustainable future (Vanholme et al., 2013). Industrial biotechnology plays a crucial role in addressing these challenges. Sustainable bioprocess technology utilizes renewable energy and raw materials instead of fossil fuels and fossil-based commodities, to produce various products, pharmaceuticals, raw materials, or energy carriers.

A bacterium of notable potential in the context of sustainable bioproduction is *Acetobacterium woodii*. This microorganism exhibits a remarkable capacity for the metabolic transformation of diverse inorganic substrates, encompassing carbon dioxide, carbon monoxide, hydrogen, a subset of C1 molecules including formate and methanol, alongside saccharides such as glucose and fructose (Bertsch & Müller, 2015; Drake et al., 2008). This metabolic versatility culminates in the synthesis of acetate as the principal end-product within its metabolic cascade.

1.2   The Objectives of the Work

The objectives of this thesis revolve around a focused investigation into the conversion of formate and the synergistic utilization of formate and CO to facilitate the bioproduction of acetate within the host organism *A. woodii*. This research was initiated with the primary intention of addressing several critical knowledge gaps in the field of microbial metabolism and bioprocess engineering, particularly in the context of acetate production through unique substrate utilization in a chemical defined medium.

The initial phase of this investigation involved a comprehensive exploration of the feasibility of various experimental conditions. To this end, a series of serum bottle experiments were designed and conducted. One of the key components was the strategic implementation of adaptive laboratory evolution to improve the host organism's performance. This approach aimed to enhancing *A. woodii's* capabilities for formate utilization and acetate production. The decision of the selection of a chemically defined growth medium was made to provide precise control over the nutrient composition and to eliminate confounding variables that could arise from the use of complex, undefined media. The performance factors were compared to a previous study with similar conditions conducted in a complex medium (Neuendorf et al., 2021).

Providing essential vitamins to support the growth and metabolic activity of *A. woodii* was another pivotal aspect of the study. Vitamins are essential for optimizing various cellular processes; however, they can be costly. Therefore, it was imperative to judiciously minimize their usage, seeking to employ only the necessary minimum quantities.

Exploring the most effective carbon source combinations and medium selection was the last consideration of this phase. The combination of formate and CO was considered to harness potential synergies between these substrates, potentially increasing the yield of acetate.

This phase of experimentation culminated in the transition to continuous cultivation experiments, a substantial shift from the batch culture conditions. Continuous bioproduction introduces a seamless and uninterrupted flow of production, resulting in higher productivity as it eliminates idle periods between batches and enables a constant feed of raw materials. This operation method ensures consistent product quality through real-time monitoring and adjustments, leading to faultless control over essential parameters. Furthermore, continuous bioproduction contributes significantly to sustainability by reducing waste generation, minimizing product losses during startup, shutdown, and cleaning. The scalability of continuous bioproduction systems offers a flexible and cost-effective pathway for expansion to meet growing demands without major process redesigns. Continuous bioproduction is economically viable as it offsets the higher initial setup costs with long-term efficiency gains. Overall, continuous

bioproduction enables online measurement and control, enhancing productivity, maintaining consistent product quality while promoting environmental sustainability.

In these bioreactor experiments, formate was exclusively utilized as the carbon and energy source. This shift was particularly significant because, historically, studies on *A. woodii* had predominantly been conducted in rich growth media, and only a limited number of studies had specifically investigated formate as a viable substrate (Moon et al., 2021; Neuendorf et al., 2021; Novak et al., 2021). The shift to continuous cultivation was motivated by the need to mimic real-world bioproduction conditions more closely and to get insights into the production, uptake, and growth rates as well as the yields.

In conclusion, the primary objectives of this work are to explore the potential of formate and CO as substrates for acetate bioproduction in *A. woodii*, while also investigating the influence of adaptive laboratory evolution, vitamin supply, and continuous cultivations in chemical defined medium. The outcomes of this research will contribute to our understanding of microbial metabolism and bioprocess engineering and may hold significant implications for sustainable bioproduction processes in the future.

1.3   Feedstock

In the realm of sustainable bioproduction, the choice of feedstock holds paramount importance. It is imperative that the selected feedstock is sourced from renewable raw materials or waste streams, aligning with the principles of environmental responsibility and resource efficiency. Presently, formic acid holds a position of promise for energy storage generated with the use of excess renewable electricity. It stands as the most elementary carboxylic acid and finds utility as a substrate in a wide array of biochemical applications (Cotton et al., 2020; Yishai et al., 2016).

Diverging from hydrogen, carbon dioxide, and carbon monoxide gases, formate possesses the advantage of being in a liquid state, thereby facilitating its handling and transportation with greater ease. Based on information provided by the European Chemical Agency, formic acid and formate exhibit a rapid biodegradation. This characteristic extends to their biodegradability within seawater environments as well (European Chemical Agency, 2023). Various alternative routes to fossil-based formate production have been explored, including electrochemical, photocatalytic CO_2 reduction, hydrogenation of carbon dioxide and hydrolysis, wet oxidation, and catalytic oxidation from biomass (Bulushev & Ross, 2018). Electrochemical methods involve the use of electricity to drive the conversion of CO_2 into formate, utilizing complex and high selective catalysts (Merino-Garcia et al., 2021). Photocatalytic CO_2 reduction employs light energy and catalysts to drive the conversion process (Adamu et al., 2023). Lastly, hydrogenation of carbon dioxide involves reacting CO_2 with hydrogen gas in the presence

of suitable catalysts to produce formate (Cannon & Saouma, 2021; Zhou et al., 2021). These alternative routes offer promising strategies to produce formate sustainably for further deployment as a substrate for biochemical conversion into valuable products.

1.4   Acetogens

A noteworthy group of bacteria displaying potential for sustainable biosynthesis includes acetogens, among which *Acetobacterium woodii* stands out as a representative genus. Acetogenic microorganisms comprise a specialized class of strictly anaerobic bacteria that are widely distributed throughout natural environments. Alongside archaea, acetogens constitute the final living beings within the anaerobic food chain. A distinctive feature of acetogens is their reliance on the Wood–Ljungdahl pathway for carbon dioxide reduction, with central involvement of the acetyl-CoA synthase enzyme (Karekar et al., 2022). This biochemical route enables their growth via chemolithoautotrophy, wherein hydrogen and carbon dioxide serve as substrates, uniquely combining carbon dioxide fixation with ATP synthesis. What sets acetogens apart from organisms employing alternative metabolic pathways is their distinctive capacity to perform reductive synthesis of acetate from carbon dioxide. This biochemical route is regarded as one of the earliest on Earth (Lemaire et al., 2020).

The significance of acetogens extends beyond their metabolic capabilities. Their unique evolutionary history and ancient lineage contribute to their importance in understanding microbial evolution and the development of early life forms. Acetogens are believed to have emerged before oxygenic photosynthesis, making them one of the oldest lineages of microorganisms on Earth. Comparative analysis of the seven identified CO_2 fixation pathways among prokaryotes reveals that the acetyl-CoA pathway stands out as one of the most ancient. The linear structure of the pathway leading to acetate suggests its ancient origin compared to the other five more complex cyclic pathways. The second known linear CO_2 fixation pathway is the reductive glycine pathway, which was the last confirmed one (Sánchez-Andrea et al., 2020). The five cyclic pathways involve several distinct intermediate molecules with specific stereochemical arrangements in their structure. In contrast, the process of combining a methyl group and carbon monoxide to form acetate do not result in the creation of chiral centers in the intermediate molecules involved in carbon dioxide fixation. Furthermore, it operates exclusively under anaerobic conditions, and it serves as a pathway for both carbon and energy metabolism. All these characteristics appear to serve as a favorable foundation for initiating evolutionary specialization, particularly when considering the conditions that prevailed on Earth during its early stages. Moreover, carbon isotope evidence, which aligns with the functioning of the acetyl CoA pathway, has been detected in rocks estimated to be 3.46

and even 3.95 billion years old (Tashiro et al., 2017; Ueno et al., 2006). This evidence suggests that the initial organisms may have relied on hydrogen and carbon dioxide from hydrothermal vents (Martin, 2020).

1.4.1 Acetobacterium woodii

Acetobacterium woodii, named in honor of Harland G. Wood, is a remarkable microorganism with unique characteristics and metabolic capabilities. In 1977 Ljungdahl and Wood first discovered and characterized *A. woodii*. The organism was isolated from black sediment from a marine estuary in Woods Hole, Massachusetts, USA. The mesophilic, anaerobic, gram-positive bacterium belongs to the clostridia class. The oval-shaped acetogen usually occurs in pairs and has a size about 1.2×2.5 µm (Balch et al., 1977; Jacob Bryde, 2014).

The WLP or acetyl-CoA pathway serves as the primary energy conservation mechanism and as the main route for acetogens to synthesize acetyl-CoA, which is essential for cellular carbon generation and the production of acetate (Karekar et al., 2022). Reducing carbon dioxide necessitates an input of energy, a requirement that can be met by introducing gaseous-phase hydrogen, which undergoes oxidation concurrently within the metabolic activity. CO_2 is introduced into the WLP via two different routes. In one route, CO_2 is reduced to formate by utilizing H_2, while in the other route, CO_2 is reduced to carbon monoxide using ferredoxin (Basen & Müller, 2017). The underlying WLP, its stoichiometry, and the associated thermodynamics will be further discussed in subsequent sections.

Furthermore, *A. woodii* exhibits exceptional versatility in its substrate utilization capabilities. In addition to CO_2, it can metabolize a wide range of organic compounds, including sugars, alcohols, carboxylic acids, and amino acids (Dönig & Müller, 2018; Litty et al., 2022). Studies have demonstrated the occurrence of growth in various conditions, including autotrophic, heterotrophic, and mixotrophic settings. Investigations have examined the combinations of CO_2 and CO with electron-donating compounds such as H_2, fructose, and formate (Cheng et al., 2018; Neuendorf et al., 2021; Steger et al., 2017; Straub et al., 2014). This metabolic flexibility allows *A. woodii* to adapt to different substrates, making it a resilient microorganism with the potential to thrive in various biotechnological applications.

1.4.1.1 Vitamin Requirement

Vitamins exhibit diverse biochemical functions, and many of them are essential for individual organisms. In the case of microorganisms, a standard mixture of various vitamins is typically employed to meet their nutritional requirements. Notably, not all

vitamins are metabolically utilized by organisms, and a significant portion may become surplus during the cultivation process.

Early investigations on *A. woodii*, conducted by Balch et al., 1977, briefly addressed the topic of nutrition alongside other factors. In their study, growth experiments were conducted using individual vitamins separately. The results of these nutrition studies suggested that pantothenate alone could fulfill the vitamin requirement for *A. woodii* (Balch et al., 1977). Pantothenate, a member of the B complex vitamins and commonly referred to as Vitamin B_5, serves as a precursor to coenzyme A. (Bender, 2003).

1.5 *The Wood-Ljungdahl pathway*

The Wood-Ljungdahl pathway is a metabolic pathway found in certain bacteria and archaea that allows them to utilize carbon dioxide as a carbon source for growth. This pathway efficiently harnesses CO_2 as a carbon source, supporting growth and metabolic activities. This pathway involves a series of enzymatical reactions that convert two molecules of CO_2 primarily into one molecule of acetyl-CoA. It consists of two branches, the methyl branch, and the carbonyl branch, which operate in parallel. In the methyl branch, CO_2 undergoes a six-electron reduction process to form methyl-THF. In the carbonyl branch, CO_2 is converted into carbon monoxide. Subsequently, CO combines with the methyl group and CoA to produce acetyl-CoA (Karekar et al., 2022).

Acetogenesis is linked to the synthesis of ATP through a membrane bound chemiosmotic process, which comprises a ferredoxin dependent ion-pump, as well as an ion-ATP synthase. In the case of *A. woodii*, the cells build up a gradient of sodium ions (Na^+) that drives this process (Poehlein et al., 2012). Figure 1 illustrates the WLP of *A. Woodii*. The underlying stoichiometric chemolithoautotrophic reaction is written in Equation 1. The three potential stoichiometric reaction equations for formate and CO consumption and the corresponding reaction Gibbs energy values, as conducted in this study, are provided in Equation 2, 3, and 4.

Equation 1: Reaction equation of acetogenesis for chemolithoautotrophy

$$4\,H_2 + 2\,CO_2 \longrightarrow CH_3COOH + 2\,H_2O \qquad \Delta_r G'^m = -99.1\,\text{kJ} \cdot \text{mol}^{-1}$$

One molecule of carbon dioxide enters the pathway through two different branches: the methyl branch and the carbonyl branch. Both branches work in parallel and merge, resulting in the formation of acetyl-CoA, an important metabolite. It can be utilized to produce biomass, which is essential for the growth and maintenance of cells. Alternatively, acetyl-CoA can be further metabolized to acetyl-phosphate. The phosphoryl group is transferred to ADP to generate energy in the form of ATP and acetate (Wood et al., 1986).
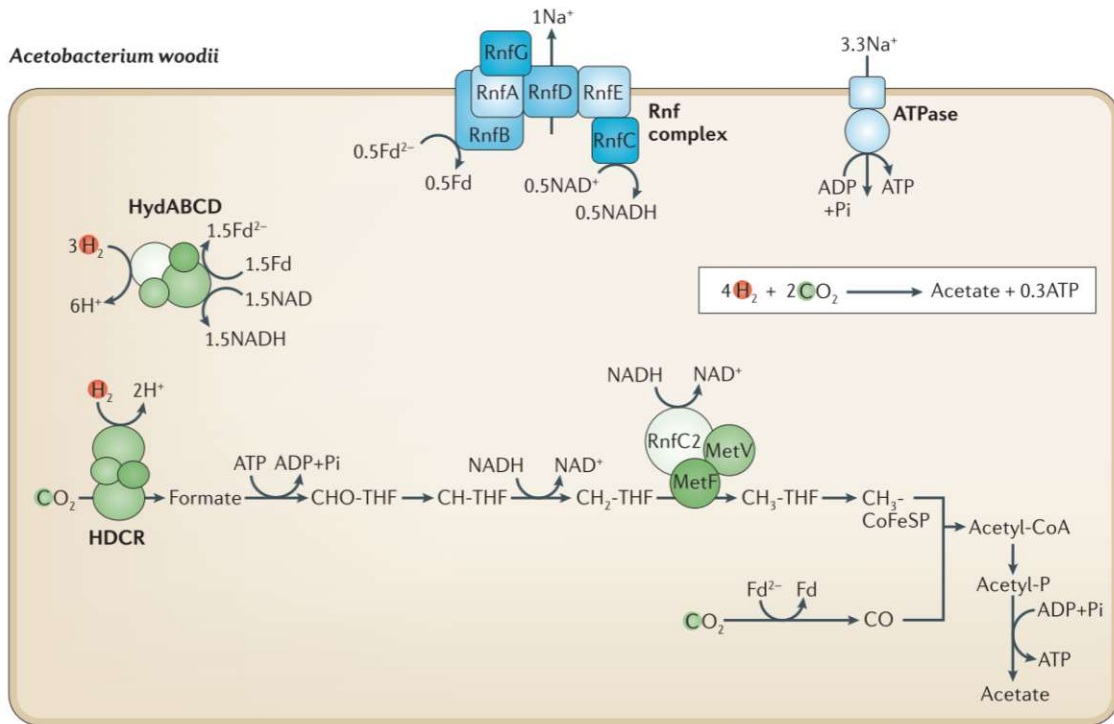
Figure 1: Model for acetogenesis in *A. woodii*. (Schuchmann & Müller, 2014b)

In the methyl branch the process begins with the two-electron reduction and hydrogenation of CO_2 to formate. This reduction is catalyzed by the enzyme complex hydrogen-dependent CO_2 reductase (HDCR) consisting of hydrogenase, formate dehydrogenase and electron transfer units (Figure 2). Schuchmann et. al., 2016 suggested that molecular hydrogen is directly oxidized by the hydrogenase subunit HydA2 and donates the electrons via electron transfer units to a formate dehydrogenase (FdhF2), which subsequently reduces CO_2 to formate (Schuchmann et al., 2016).
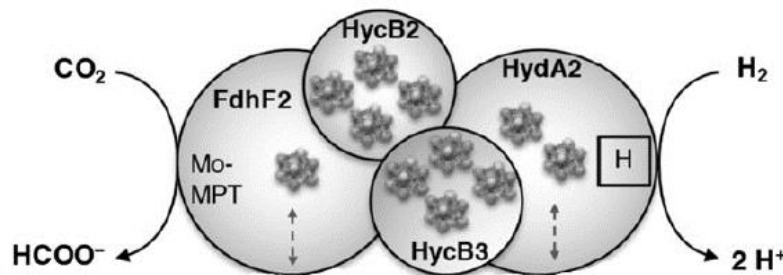
Figure 2: HDCR complex. The HDCR of *Acetobacterium woodii* is a heterotetramer catalyzing hydrogen-dependent reduction of CO_2 (Schuchmann et al., 2016).

The subsequent stage in the methyl branch involves the reaction of formate with THF, facilitated by ATP, resulting in the formation of 10-formyl-THF. This chemical transformation is carried out by an enzyme known as 10-formyl-THF synthetase. The following two steps in the pathway are mediated by two different enzymes: 5,10-methenyl-THF cyclohydrolase and 5,10-methylene-THF dehydrogenase. Initially, the formyl group undergoes reduction to methenyl THF. The subsequent reduction step, leading to methylene-THF, relies on the presence of NAD in *A. woodii*, whereas various other microorganisms exhibit a dependency on NADP for this reaction (Ragsdale & Pierce, 2008).

In the carbonyl branch, the first step involves the activation of CO_2. This is achieved through the action of an enzyme called carbon monoxide dehydrogenase (CODH). CODH catalyzes the reaction where CO_2 is converted into carbon monoxide and water. The CO binds to Ni, the active site of CODH. This thermodynamical unfavored reduction is driven by the oxidation of negatively charged ferredoxin. The last step of the WLP is catalyzed by the enzyme acetyl-CoA synthase (ACS). ACS combines the methyl group with coenzyme A and the carbonyl group. This step completes the merging of the methyl and carbonyl branches, leading to the production of acetyl-CoA, which is a central metabolite used for various cellular processes. The resulting acetyl-CoA can be further utilized for biomass production, energy generation combined with acetate production, and the synthesis of important molecules (Ragsdale & Pierce, 2008).

Acetogens exhibit distinct energy metabolism patterns, classifiable into two primary groups. One group is equipped with cytochromes and quinones, which participate in a membrane-bound electron transport process, ultimately generating a H^+ gradient across the membrane. These organisms harness this proton potential to operate ATP synthase (Müller, 2003).

In contrast, the second group, exemplified by the Gram-positive bacterium *Acetobacterium woodii*, follows a more ancient iteration of the energy metabolism pathway (Poehlein et al., 2012). This variant relies on at least one ion pump, specifically a sodium ion-translocating ferredoxin:NAD^+ oxidoreductase (Rnf). The Rnf complex is a membrane-bound electron transfer system featuring iron-sulfur centers and flavins (Biegel & Müller, 2010). In the context of *A. woodii*, it was observed that exergonic electron transfer from reduced ferredoxin to NAD^+ correlates with vectorial Na^+ transport through the membrane vesicles (Hess et al., 2013).

This reliance on sodium ion potential is a distinctive characteristic of *A. woodii*. The sodium ion gradient across the membrane plays a pivotal role in driving ATP synthesis via a membrane-integrated Na^+ F_1F_O ATP synthase (Imkamp & Müller, 2002).

1.5.1 Stoichiometry and Thermodynamics

In this study, CO_2 was not used as a substrate, but formate and carbon monoxide were employed instead. However, the metabolic pathways proceed in a very similar manner. First, the use of formate as the sole substrate is described.

Formate can be directly converted into formyl-THF in the methyl branch. The formate dehydrogenase in the HDCR complex acts in reverse order, oxidatively converting formate. This process generates CO_2 and hydrogen. The hydrogen, in turn, serves as an energy supplier through the reduction of NAD^+ and Fd. Subsequently, the remaining steps of the previously described WLP can be carried out. The CO_2 produced during formate oxidation is also required for the carbonyl branch (Moon et al., 2021; Schuchmann & Müller, 2012).

The stoichiometric equation depicting the conversion of formate to acetate can be deconstructed into two distinct redox equations. In the initial oxidation equation, the transformation of 3 moles of formate yields 3 moles of CO_2, accompanied by the generation of 6 electrons and 6 protons. The subsequent reduction equation involves the interaction of 1 mole of formate and 1 mole of carbon dioxide, utilizing 6 electrons and 6 protons to synthesize 1 mole of acetate and 2 moles of water. Consequently, a cumulative total of 4 moles of formate is necessitated for the biogenic synthesis of 1 mole of acetate.

Before formate reduction can occur, it must undergo oxidation at the HDCR complex, generating CO_2 and a proton donor such as H_2, NAD(P)H, or Fd^{2-}. Once a sufficient amount of energy carriers is produced, a transition to formate and CO_2 reduction takes place. However, during the growth phase, formate must also be oxidized to sustain the production of H_2, NAD(P)H, and Fd^{2-} (Schuchmann & Müller, 2013).

Equation 2: Reaction equation for the conversion of formate towards acetate.

$$3\ HCOOH \longrightarrow 3\ CO_2 + 6\ e^- + 6H^+$$

$$HCOOH + CO_2 + 6\ e^- + 6H^+ \longrightarrow CH_3COOH + 2\ H_2O$$

$$4\ HCOOH \longrightarrow 1\ CH_3COOH + 2\ H_2O + 2\ CO_2 \qquad \Delta_r G'^m = -82.1\ kJ \cdot mol^{-1}$$
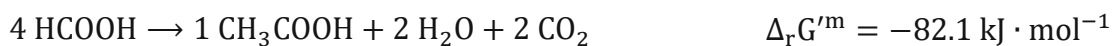
In the case of a mixture of formate and CO, formate must still be oxidized to CO_2 in order to obtain energy and H_2 for all possible metabolic activities. Stoichiometric investigations yield two possible reaction pathways.

In the first scenario, CO can be built in as a carbonyl group solely acting as a carbon source. In this pathway, only 2 formate molecules need to be oxidized to reduce 1 formate together with 1 CO, resulting in the production of acetate. Consequently, the synthesis of 1 acetate would demand 3 formate molecules and 1 carbon monoxide.

Equation 3: Reaction equation for the conversion of formate and CO towards acetate. Pathway 1

$$2\ HCOOH \longrightarrow 2\ CO_2 + 4\ e^- + 4\ H^+$$

$$HCOOH + CO + 4\ e^- + 4\ H^+ \longrightarrow CH_3COOH + H_2O$$

$$3\ HCOOH + CO \longrightarrow CH_3COOH + H_2O + 2\ CO_2 \qquad \Delta_r G'^m = -113.8\ kJ \cdot mol^{-1}$$
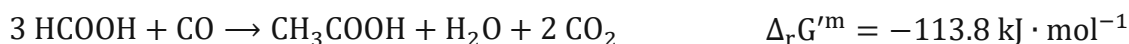
In the second pathway, CO can be oxidized while simultaneously reducing Fd, allowing it to serve as both a carbon and electron source. In this case, the reduction of 1 formate with 1 CO to produce 1 acetate would necessitate the oxidation of 2 CO molecules. Hence, the synthesis of 1 acetate would demand 1 formate molecule and 3 CO molecules (Bertsch & Müller, 2015).

Equation 4: Reaction equation for the conversion of formate and CO towards acetate. Pathway 2

$$2\ CO + 2\ H_2O \longrightarrow 2\ CO_2 + 4\ e^- + 4\ H^+$$

$$HCOOH + CO + 4\ e^- + 4\ H^+ \longrightarrow CH_3COOH + H_2O$$

$$HCOOH + 3\ CO + H_2O \longrightarrow CH_3COOH + 2\ CO_2 \qquad \Delta_r G'^m = -177.3\ kJ \cdot mol^{-1}$$

A. woodii possesses two hydrogenase enzymes that are involved in H_2 oxidation, both of which are highly susceptible to inhibition by CO. One of these enzymes is an electron-bifurcating hydrogenase (HydABCD), which reduces ferredoxin and NAD^+ (Schuchmann & Müller, 2012). The second hydrogenase is part of the HDCR complex, responsible for reducing CO_2 to formate using H_2 or Fd^{2-} as electron donors. In the presence of gaseous carbon monoxide at concentrations of at least 10 %, the utilization of reduced ferredoxin becomes the sole viable option, owing to the inhibition of the hydrogenase component within the HDCR complex (Schuchmann & Müller, 2013). Analysis of CO inhibition, as determined through measurements on purified enzymes, reveals that the bifurcating hydrogenase is approximately twice as sensitive to CO inhibition as the HDCR component (Bertsch & Müller, 2015). Consequently, the presence of CO is expected to inhibit formate production via the HDCR complex from CO_2, leading to a bottleneck in the initial step of the methyl branch of the Wood-Ljungdahl pathway. Therefore, different concentrations of CO were tested in combination with formate to demonstrate this inhibitory effect.

When CO is used as the sole substrate, its oxidation by CODH generates reduced ferredoxin, which can be utilized at the Rnf complex to transport Na^+ ions out of the cell while reducing NAD^+. Furthermore, the reduced ferredoxin (Fd^{2-}) can potentially serve as an electron donor for CO_2 reduction to formate via the HDCR complex. This phenomenon was elucidated by Schuchmann and Müller 2013 using purified HDCR and CODH enzymes rather than employing active bacterial cultures. Furthermore, their

investigation revealed that the efficacy of ferredoxin as an electron donor was significantly lower, approximately 20-fold less, when compared to hydrogen (Schuchmann & Müller, 2013).

Additionally, studies have demonstrated that the presence of CO in combination with CO_2 and H_2 led to inhibited growth in *A. woodii*. It was found that higher CO concentrations (above 3 %) resulted in slower H_2 consumption compared to systems without CO addition. Consequently, cells required a longer time to grow due to the inhibitory effects imposed by CO (Bertsch & Müller, 2015).

2   Material and Methods

2.1   Bacterial Strain

The bacterial strain of *Acetobacterium woodii* was sourced from the laboratory's culture collection, subcultured for adaptation and optimization, the details of which are comprehensively expounded upon in Chapter 3.1 of this thesis. The cell cultures were stored in cryogenic storage vials at -80 °C. For this, they were mixed anaerobically with saccharose with a final concentration of 125 g L^{-1}. All experiments were performed with adapted cells from the mentioned strain.

2.2   Medium Preparation

The medium was prepared for shaken cultivation in serum bottles, for batch and for continuous cultivation in the bioreactor. Cells were ether grown on a chemical defined phosphate or carbonate buffered medium for serum bottle cultivation. The pH of all shaken cultivation medium was adjusted to 6,8 with 2 M H$_2$SO$_4$ / 5 M KOH while the pH value in the bioreactor was kept constant at 7 by adding 2 M H$_3$PO$_4$ unless stated otherwise. The composition of all used media is shown in Table 1 and Table 2. In all reactor experiments the phosphate buffered CDM was used.

Table 1: Chemical composition of the phosphate buffered medium.

Phosphate buffered Medium

Salt solution:

NaCl	3.4	g L^{-1}
NH$_4$Cl	1	g L^{-1}
MgSO$_4$ · 7 H$_2$O	100	mg L^{-1}
Na$_2$SeO$_3$ · 5 H$_2$O	0.194	mg L^{-1}
Na$_2$Wo$_4$ · 2 H$_2$O	0.192	mg L^{-1}

Phosphate solution (serum bottle/bioreactor):

KH$_2$PO$_4$	1.76/0.45	g L^{-1}
K$_2$HPO$_4$	8.44/0.33	g L^{-1}

Iron Solution:

FeSO$_4$ · 7 H$_2$O	26.9	µg L^{-1}

Resazurin solution:

Sodium resazurin (0.2% w/v)	0.5	mL L^{-1}

Cystein:

L-Cystein HCl · 1 H$_2$O	0.5	g L^{-1}

Trace element solution DSMZ135	40	mL L^{-1}
Adapted vitamin solution DSMZ135	20	mL L^{-1}

Table 2: Chemical composition of the carbonate buffered medium.

Carbonate buffered Medium	
Salt solution:	
NaCl	0.02 g L^{-1}
NH$_4$Cl	1 g L^{-1}
MgSO$_4$ · 7 H$_2$O	160 mg L^{-1}
CaCl$_2$ · 2 H$_2$O	2.7 g L^{-1}
Na$_2$SeO$_3$ · 5 H$_2$O	0.194 mg L^{-1}
Na$_2$Wo$_4$ · 2 H$_2$O	0.192 mg L^{-1}
Phosphate solution:	
KH$_2$PO$_4$	0.45 g L^{-1}
K$_2$HPO$_4$	0.33 g L^{-1}
Carbonate buffer:	
NaHCO$_3$	10 g L^{-1}
Resazurin solution:	
sodium resazurin (0.2% w/v)	0.5 mL L^{-1}
Cystein:	
L-Cystein HCl · 1 H2O	0.5 g L^{-1}
Trace element solution DSMZ135	20 mL L^{-1}
Adapted vitamin solution DSMZ135	20 mL L^{-1}

The composition of the trace element solution as well as the adapted and original vitamin solution DSMZ 135 is listed below (Table 3). The amount of trace elements and vitamins were doubled (Ca-pantothenate 20 times higher) in phosphate buffered medium compared to the ACETOBACTERIUM MEDIUM suggestion DSMZ 135. In selected experiments, a vitamin solution comprising solely D-Ca-Pantothenate was employed at a consistent concentration of 50 mg L^{-1}, resulting in a final concentration of 1 mg L^{-1} within the medium.

Table 3: Trace element and vitamin solution regarding to DSMZ 135.

Trace element solution DSMZ 135

	[g L^{-1}]
Nitrilotriacetic acid	1.5
$MgSO_4 \cdot 7\ H_2O$	3
$MnSO_4 \cdot 1\ H_2O$	0.5
NaCl	1
$FeSO_4 \cdot 7\ H_2O$	0.1
$Co(II)Cl_2 \cdot 6\ H2O$	0.152
$CaCl_2 \cdot 6\ H_2O$	0.1
$ZnSO_4 \cdot 7\ H_2O$	0.18
	[mg L^{-1}]
$CuSO_4 \cdot 5\ H_2O$	10
$KAl(SO_4)_2 \cdot 12\ H_2O$	20
H_3BO_3	10
$Na_2MoO_4 \cdot 2\ H_2O$	10
$Ni(II)SO_4 \cdot 6\ H_2O$	33.1
$Na_2SeO_3 \cdot 5\ H_2O$	0.3
$Na_2WO_4 \cdot 2\ H_2O$	0.4

Vitamin solution DSMZ 135

	adapted	original
	[mg L^{-1}]	
Biotin	2	2
Folic acid	2	2
Pyridoxine-HCl	10	10
Thiamine-HCl	5	5
Riboflavin	5	5
Nicotinic acid	5	5
D-Ca-pantothenate	**50**	5
Vitamin B$_{12}$	0.1	0.1
p-Aminobenzoic acid	5	5
Lipoic acid	5	5

In order to create anaerobic conditions in serum bottles, the aerobically mixed medium is purged with nitrogen gas at a flow rate of 0.4 l$_n$ min^{-1} for a minimum of 15 minutes. Following the addition of the appropriate quantity of cysteine, the medium is purged with nitrogen for another 15 minutes until a color change from blue to pink is observed, indicating the reduced form of resazurin. A bottle top dispenser is then placed on the Schott bottle, and gas flushing needles are inserted into the serum flasks. The desired amount of medium is then filled into the flasks, and the bottles are immediately sealed using a crimp cap with septa and a crimper after flushing for an additional minute. The remaining oxygen in the headspace and liquid is reduced over a period of hours or immediately following autoclaving of the serum bottle. Once the bottle is anaerobic, the

liquid changes from pink to colorless, indicating the final reduction step of the resazurin redox reaction. Right before inoculation the vitamin solution and the carbon source were added.

The bioreactor was initially treated with citric acid, rinsed with deionized water, and subsequently filled with medium prior to autoclaving. Following sterilization, the reactor was connected to all necessary pipes and the stirrer. Nitrogen was introduced while stirring and after 15 minutes, cysteine was added. The vitamins and carbon source were then added once the solution became colorless, and the batch phase was initiated by inoculation.

The feed medium was not autoclaved, but instead pumped through a sterilized filter. Vitamins and a carbon source (in all experiments, formate) were added in the first step. The mixture was then placed in a 20-liter plastic bottle and sealed tightly to be flushed with nitrogen. After 30 minutes, cysteine was added, and the mixture was sparged for an additional hour. The gas pipe was then switched from directly entering the liquid to the headspace. The pipe inside the medium was connected to a sterilized filter, which was then connected to a 10-liter anaerobic Schott bottle that had been autoclaved. The headspace of the plastic bottle was pressurized to 0.5 bar with nitrogen, which caused the overpressure to pump the medium through the filter and into the sterilized, oxygen-free feed bottle. This setup can handle a flow rate of 6 liters per hour. One advantage of this setup is the ability to change the feed while conducting continuous cultivation. Additionally, it is possible to change formate concentration by applying mass balances for the remaining feed volume and adding new medium accordingly.

In the context of creating anaerobic conditions, cysteine is added to the medium and acts as a reducing agent to remove oxygen from the system. Cysteine can bind with oxygen through a process known as oxidative coupling, by which two moles of cysteine react with half a mole of oxygen to yield one mole of cystine and water.

2.3   Growth Conditions

For batch cultivation and adaptive laboratory evolution (ALE) 125 mL serum bottles with a diameter of 54 and a height of 107 mm were used and filled with 20 mL medium. Pre cultures were grown in 500 mL serum bottles with a diameter of 75 and a height of 190 mm were used and filled with 120 mL medium. The vitamins and the desired amount of K-formate was added from a 5 M stock inside the anaerobic tent right before inoculation of 5 to 10 % depending on the final OD of the previous culture took place. The headspace was flushed for one minute with nitrogen or a mixture of N_2/CO and filled at an over pressure of 1 bar. After sampling the headspace gas mixture was renewed. For some cultivation experiments and pre cultures yeast extract was used with a concentration of 2 g L^{-1}. All bottles were incubated at 30 °C and 100 rpm in a rotary shaker.

Continuous cultivations were carried out in a 1.5 L Applikon Bioreactor system (Getinge AB, Göteborg, Sweden). Cultivations were conducted with a filling volume of 600 mL and an agitation rate of 150 rpm. During the batch phase, the stirrer speed was reduced. The temperature for all cultivations was maintained at 30 °C. The reaction volume was maintained at a constant level using a dip tube and LAMBDA PRECIFLOW peristaltic pumps (LAMBDA Instruments GmbH in Baar, Switzerland). The medium was continuously sparged with nitrogen at a rate of 0.1 vvm. The pH level was maintained at 7.0 using 2 M phosphoric acid. The offgas from the reactor was analyzed online using CO_2 and H_2 sensors (BlueSens gas sensor GmbH in Herten, Germany). For sampling, 10 mL (5 mL preliminary sample and 5 mL main sample) of cell suspension are taken from the reactor. The preliminary sample was discarded while the main sample was transferred to a Falcon tube. The sample was taken with a syringe through a self-closing valve at the sample port. 1 mL each was pipetted into three photometer cuvettes for OD measurements. 1.9 mL being filled in a 2 mL Eppendorf Safe Lock Tube. Biomass separation was achieved through centrifugation of the tube at 14,000 rpm for 10 minutes. The supernatant was kept in a -18 °C freezer until HPLC analysis. The process was monitored and controlled using Lucullus® Process Information Management System.
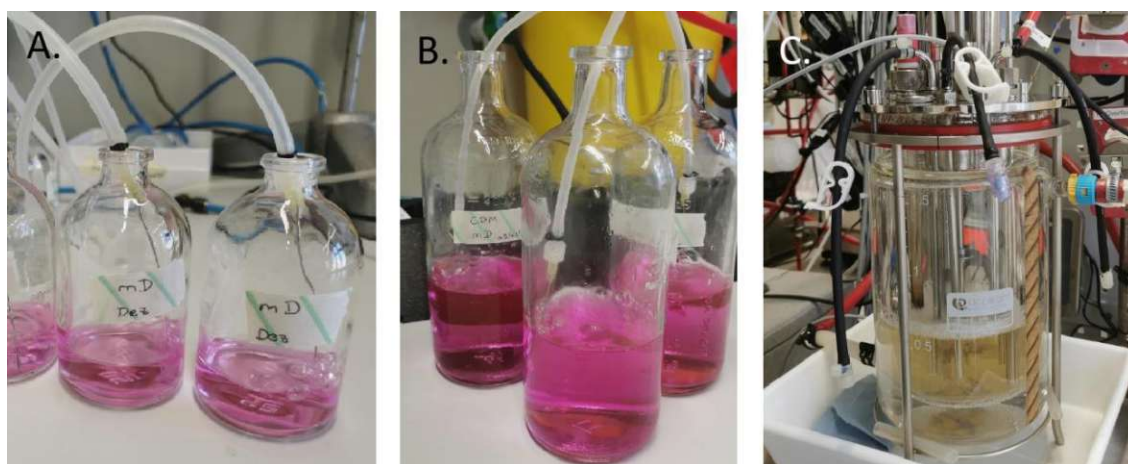
Figure 3: **A.**: Preceding autoclaving, 125 mL serum bottles undergo nitrogen (N_2) flushing to establish anaerobic conditions. **B.**: Preceding autoclaving, 500 mL serum bottles undergo nitrogen (N_2) flushing to establish anaerobic conditions. **C.**: 1.5 L Applikon Bioreactor during continuous bioproduction.

2.4 Optical Density, HPLC and Dry Cell Weight Analysis

For all OD measurements a pipette is used to transfer 1 mL of the sample into a cuvette. All samples were analyzed at the standard wavelength of 600 nm for biomass detection and additionally at 660 nm to minimize the background noise from the resazurin indicator. A Spectrophotometer ONDA V-10 PLUS was used.

All organic acids (formic and acetic acid) and sugars (glucose and fructose) were analyzed in an Ultimate 3000 High Performance Liquid Chromatograph (Thermo

Scientific, Waltham/MA, USA). The samples were prepared as follows: At first the supernatant was thawed at room temperature. 540 μL supernatant was mixed with 60 μL of a 40 M H2SO4 stock. The aimed concentration of 4 mM corresponds to the eluent concentration. The mixture was centrifuged at 14,000 rpm for 10 minutes to avoid any precipitation or biomass inside the HPLC column. After centrifugation 550 μL was carefully transferred into a HPLC vial. The calibration standards of glucose, fructose, lactate, formate, and acetate were treated the same way. Milli-Q water was directly transfered into the vial. Control, monitoring, and evaluation of the analysis was performed with Chromeleon Chromatography Data System. An Aminex HPX-87H column (300 × 7.8 mm, Bio Rad, Hercules/CA, USA) was used for all quantifications. The used eluent was 4 mM H_2SO_4 solution, and the column temperature and flow were set to 60 °C and 0.6 mL^{-min}, for 20 min. Detection was performed with a refractive index and a diode array detector.

To determine the dry cell weight under steady state conditions, 3 x 50 mL of culture broth collected after a 16-hour harvest period, during which the system parameters remained constant, were placed in Falcon tubes. After centrifuging the tubes for 10 minutes at 4 °C and 8000 rpm, they were washed with 20 mL of distilled water and centrifuged again. The resulting biomass was then carefully resuspended with 2 mL of $_dH_2O$ and transferred into pre-weighed glass tubes. These samples were dried at 120 °C for 24 hours, cooled in a desiccator for at least 1 hour, and finally weighed. The biomass concentrations at all other points were estimated using a correlation coefficient between OD_{600} and DCW (biomass = 0.38 · OD_{600}) that was determined before (Neuendorf et. al. 2021).

2.5 Calculations and Balancing

The underlying concept of all rate and yield calculations is a general material balance for a bioprocess. The material balance consists of all mass flows through the system boundaries, the biochemical reaction inside the described system and the resulting accumulation or decumulation thereof. The general material balance (Eq. 5) is also illustrated in Figure 4.

Equation 5: General Material Balance for component i.

$$\dot{V}_{In} \cdot c_{i,In} - \dot{V}_{Out} \cdot c_{i,Out} + V_R \cdot r_i = V_R \cdot \frac{\partial c_i}{\partial t} + c_i \cdot \frac{\partial V_R}{\partial t}$$

Where $\dot{V}$ is the volumetric in or out flowrate [L h^{-1}], c_i is the concentration [mol L^{-1}] of the component i, V_R is the reactor volume [L], r_i is the reaction rate [mol L^{-1} h^{-1}] of the component i and t is the time [h].
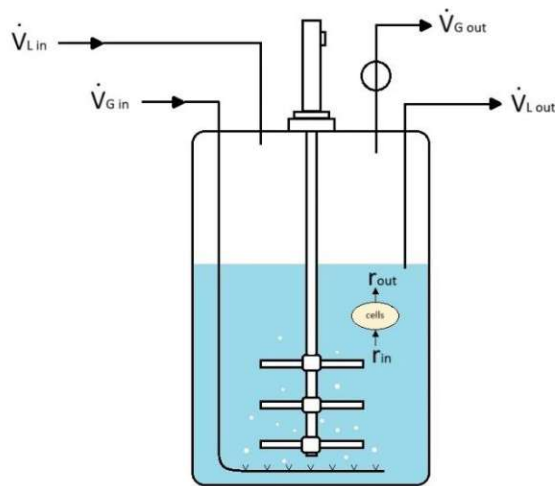
Figure 4: Schematic overview of inlet and outlet flows of the continuous bioreactor process.

Overall, simplifying the equation helps to facilitate the process, which is crucial for understanding the performance and optimization of the chemostat process. For all experiments the used substrates are K-formate and carbon monoxide. The only product is acetate. As a byproduct, CO_2 and H_2 are generated.

The general material balance for biomass in a batch process can be simplified as follows.

Equation 6: Material balance for biomass in a batch process.

$$V_R \cdot r_X = V_R \cdot \frac{\partial\, c_X}{\partial\, t}$$

The ratio of the volumetric reaction (production or uptake) rate to the biomass concentration is defined as the specific reaction (production or uptake) rate. $q_i = \frac{r_i}{c_X}$

It is common that the specific biomass production rate q_X is called specific growth rate and written as µ. Integration with the initial condition $c_X(0) = c_{Xo}$ and transformation to µ of Eq. 6 leads to the calculation of the specific growth rate during a batch process.

Equation 7: Growth rate during a batch process.

$$\mu = \frac{ln\left(\frac{c_X}{c_{X0}}\right)}{t}$$

The doubling time is reached when the biomass concentration is twice as high as the initial concentration ($c_X = 2 \cdot c_{X0}$).

Equation 8: Doubling time during a batch process.

$$t_D = \frac{ln(2)}{\mu} = \frac{0.693}{\mu}$$

The number of generations is intrinsically linked to the doubling time, where each doubling time corresponds to one generation. However, in practice, the specific growth rate and thus the doubling time is only constant during the logarithmic growth phase. Therefore, it is feasible to calculate the number of generations by determining the initial and final biomass concentrations.

$$c_{X0} \cdot 2^n = c_X$$

After logarithmic transformation, the number of n-generations can be expressed using the following equation.

Equation 9: Number of generations in batch processes.

$$n = \log_2\left(\frac{c_X}{c_{X0}}\right) = \frac{\log\left(\frac{c_X}{c_{X0}}\right)}{\log(2)} = 3.32 \cdot \log\left(\frac{c_X}{c_{X0}}\right)$$

In the chemostat process, it is essential to calculate the material balances for substrates, products, and biomass accurately. In all chemostat experiments formate were used as the sole substrate. To this end, the equation of material balances can be simplified as follows. The volumetric inlet and outlet flow is equal and set at a constant rate. This rate is further expressed as the dilution rate [h^{-1}], which describes the flow per reactor volume.

$$D = \frac{\dot{V}}{V_R}$$

The reciprocal value describes the time of one volume change. The calculation of biomass and acetate production rates is always conducted between two consecutive measuring points.

Equation 10: Growth rate for chemostat

$$r_X = \frac{\Delta c_X}{\Delta t} + D \cdot c_X$$

Equation 11: Formate uptake rate for chemostat

$$r_{For} = \frac{\Delta c_{For}}{\Delta t} + D \cdot \left(c_{For,In} - c_{For,Out}\right)$$

Equation 12: Acetate production rate for chemostat

$$r_{Ace} = \frac{\Delta c_{Ace}}{\Delta t} + D \cdot c_{Ace}$$

Equation 13: Carbon evolution rate for chemostat

$$r_{CO_2} = CER = \frac{\dot{V}_{G,In}}{V_R} \cdot c_{CO_2} = \frac{\dot{V}_{G,In}}{V_R} \cdot \frac{\varphi_{CO_2}}{V_M}$$

Equation 14: hydrogen evolution rate for chemostat

$$r_{H_2} = HER = \frac{\dot{V}_{G,In}}{V_R} \cdot c_{H_2} = \frac{\dot{V}_{G,In}}{V_R} \cdot \frac{\varphi_{H_2}}{V_M}$$

$\dot{V}_{G,In}$ is the inlet gas flow of pure nitrogen. The gas flow rate was set to 0.1 vvm, which corresponds to 0.058 sL min^{-1} at 20 °C and 1 atm (standard conditions). The concentration of CO_2 and H_2 can be calculated using the BlueSense off-gas sensors. The digital value they provide represents the volumetric fraction [φ_i]. The molar concentration can be determined using the molar volume at standard conditions.

$$V_M = \frac{R \cdot T}{p} = 24.05 \, \frac{sL}{mol}$$

R is the molar gas constant [L Pa K^{-1} mol^{-1}], T the temperature [K], and p the pressure [Pa].

In order to compare fermentation processes more effectively, the volumetric rates are related to the biomass concentration, resulting in specific rates [g$_i^{-1}$ g$_x^{-1}$ h^{-1}]. The substrate-associated yield is of considerable scientific interest. The examination of the stoichiometric equation for the conversion of formate, as the exclusive carbon substrate, into acetate, shows a maximum chemical yield of 0.250 mol mol^{-1}, stemming from the fact that 4 moles of formate yield 1 mole of acetate (Eq. 2). The calculation of the yield is executed as described below.

Equation 15: Acetate Yield calculation

$$Y_{Ace/For} = \frac{r_{Ace}}{r_{For}}$$

With a view to verify the process, and specifically the reaction rates, a carbon balance around the cell is considered. This involves examining the reaction equation and using the calculated C-molar reaction rates as stoichiometric factors. The C-molar mass is obtained by dividing the molar mass by the number of carbon atoms in the molecule. To estimate the C-molar biomass, a carbon content of 45 w% is assumed (Godley et al., 1990). Since all reaction rates are accessible, the system is considered determined. By dividing the left-hand side of the equation by the right-hand side, the result should be 1 or 100%. This approach allows for better comparison of fermentation processes and provides insight into the efficiency of carbon utilization.

In the context of electrochemical reactions, each molecule has a Degree of Reduction (DoR) that is determined by its capacity to either donate or receive electrons. This value represents the number of electrons that an electron donor can contribute, or an electron acceptor can assimilate per mole of the compound. Notably, the DoR for any element within a compound is identical to the valence of that specific element.

Furthermore, within the domain of bioprocess engineering, the DoR is symbolized as γ and is explicitly defined as the quantity of equivalent electrons available per mole of carbon atoms within the compound. As an illustration, consider the DoR for acetate (H_3CCOO^-). This calculation involves summing up the valence electrons for each atom: 4 electrons per carbon (C), 1 electron per hydrogen (H), -2 electrons per oxygen (O), and an additional electron to account for the negative charge. The summation yields a total of 8 electrons. Given that acetate contains two carbon atoms, this value is subsequently divided by 2 to maintain a balanced representation per carbon, resulting in a final of 4 e^-/C-molar. An assumed Degree of Reduction (DoR) of 4.15 moles of electrons per mole of carbon was attributed to *A. woodii* (Neuendorf et al., 2021).

Equation 16: Degree of Reduction Balance for a general chemical equation.

$$\sum_{Educts} \gamma_i \cdot r_i = \sum_{Products} \gamma_j \cdot r_j$$

3   Results and Discussion

This thesis presents a comprehensive analysis of the anaerobic biosynthesis by *A. woodii* of formate and CO to produce acetate as the sole product. The investigation covers several crucial aspects of this process, including strain selection through adaptive laboratory evolution, media selection, the influence of vitamins, different growth conditions in serum bottles based on substrate availability, the characterization of steady states at various dilution rates and formate concentrations, and observations and challenges in continuous fermentation.

Strain selection through adaptive laboratory evolution represents a powerful strategy for enhancing the performance of microorganisms in desired metabolic pathways. This section discusses the methodology and outcomes of the evolutionary process aimed at identifying strains with improved growth rates and acetate production capabilities.

To ensure successful implementation of this process, the selection of an appropriate growth medium is crucial. This section presents the results obtained from two different media formulations, analyzing their impact on the biomass growth rate and final optical densities.

Furthermore, the influence of vitamins on growth is examined, as these essential nutrients are known to play a critical role in microbial metabolism. The results shed light on the specific vitamin requirements and their impact on the productivity of the biosynthetic pathway.

To explore the impact of different growth conditions, variations in substrate availability are investigated. By altering the concentration and ratios of formate and CO, valuable insights are gained regarding the system's response and the potential limitations encountered under different conditions.

The characterization of steady states at different dilution rates and formate concentrations in continuous cultures providing insights into the system's stability, productivity, efficiency, and robustness under different operating conditions. These outcomes were compared to the study by Neuendorfer et. al. 2021.

Lastly, the challenges associated with continuous fermentation and maintaining steady-state conditions are also explored in this thesis. The observations made during continuous fermentation experiments provide valuable information on the system dynamics, limitations, and potential optimization strategies for sustained acetate production.

3.1   Genealogy and Adaptive Laboratory Evolution

The genealogy throughout the entire duration of this study is visually represented by the following two figures (Figure 5 and 6). A comprehensive description is provided below. It should be noted that these figures do not present a complete depiction of all conditions, as numerous unsuccessful experiments have been excluded but will be explained later.

. The process of adaptive laboratory evolution is segmented into four stages. The initial phase involves the adaptation to formate and carbon monoxide cultivation in a chemically defined medium. Subsequently, the focus shifts to the selection of the optimal growth medium and the assessment of various substrate concentrations. However, experiments with variable vitamin supplies led to the simultaneous cessation of growth across all tested conditions. As a result, the cultivation process recommenced using a previously cryopreserved culture, successfully enabling the determination of vitamin requirements and the adaptation of the strain to utilize formate as the sole carbon source, with the ultimate aim of employing it in continuous bioreactor cultivation.
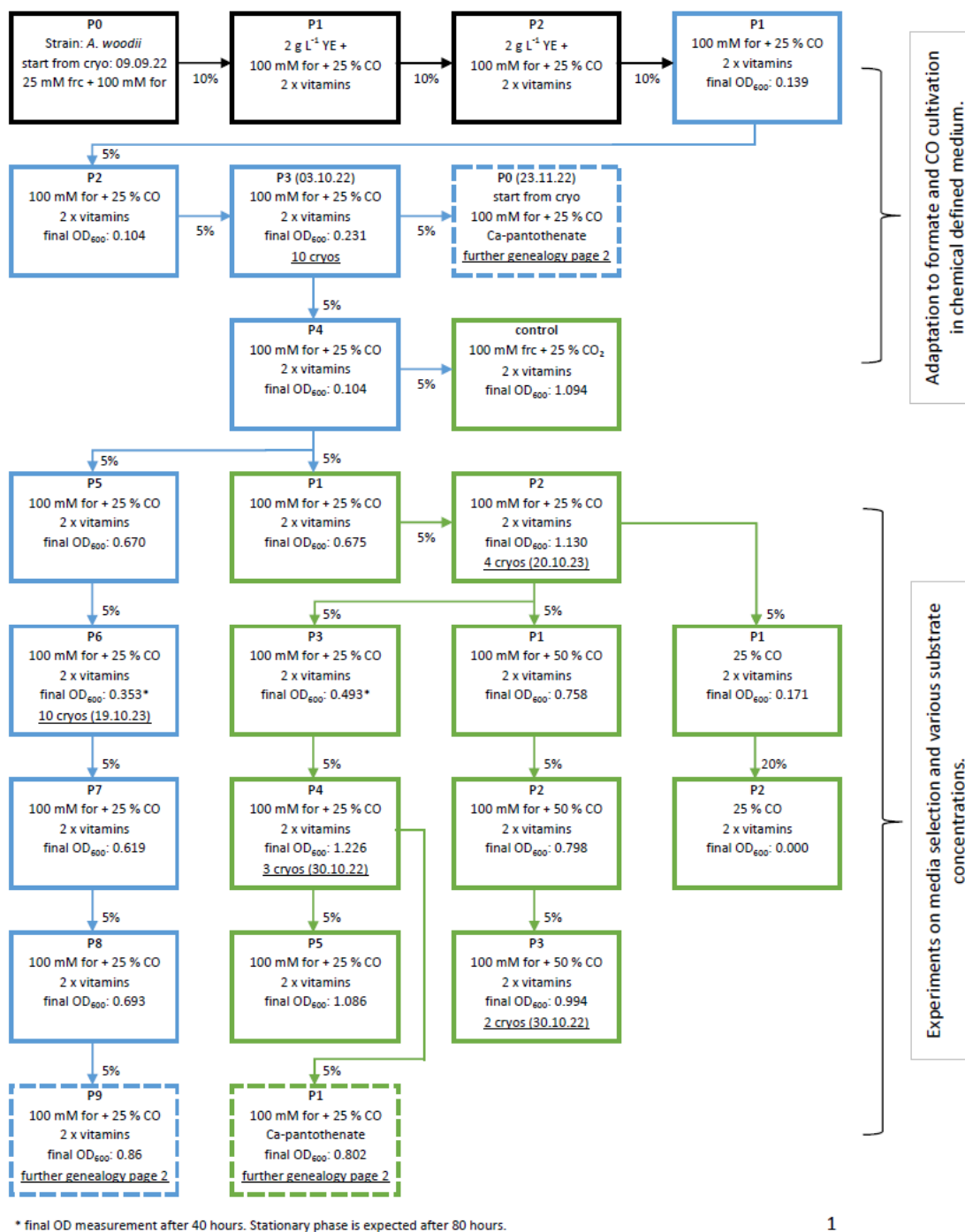
Figure 5: Genealogy Part 1. The boxes outlined in black represent a rich phosphate buffered medium, while the blue and green boxes represent chemically defined phosphate and carbonate buffered media, respectively. The percentage values indicated at the arrows describe the inoculum amount. The final biomass concentration was measured between 75 and 90 hours.
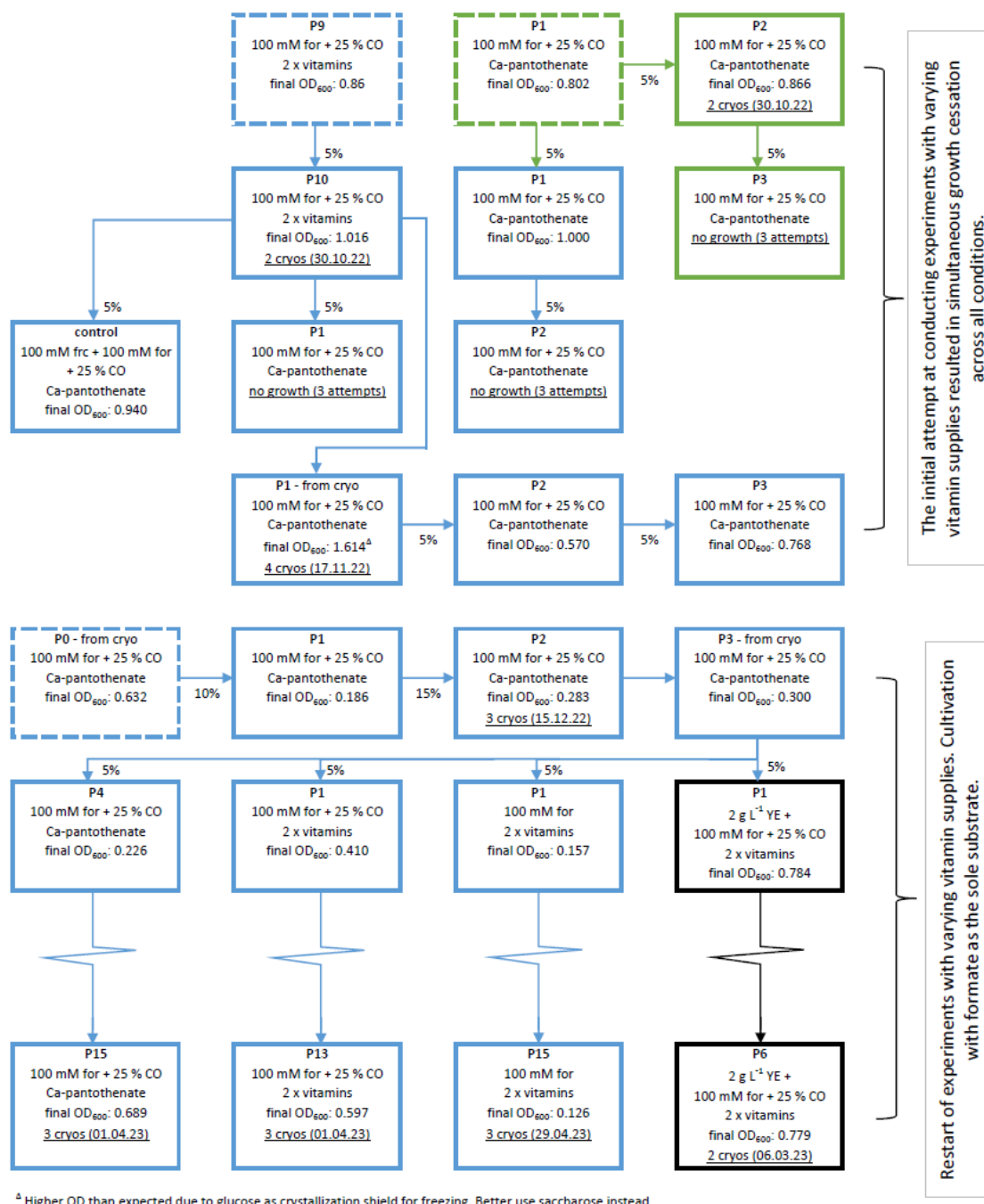
Figure 6: Genealogy Part 2. The boxes outlined in black represent a rich phosphate buffered medium, while the blue and green boxes represent chemically defined phosphate and carbonate buffered media, respectively. The percentage values indicated at the arrows describe the inoculum amount. The final biomass concentration was measured between 75 and 90 hours.

Initially, a mixture of fructose and formate served as the carbon and energy source. In subsequent iterations, fructose was replaced with gaseous carbon monoxide. Later, the addition of yeast extract was omitted, resulting in a final optical density of 0.139 observed in the first successful culture. Following two additional passages, 10 cryo stocks were generated. In the 10th passage within this specific environment, the maximum optical

density recorded was 1.016. This value represents the highest OD_{600} achieved in phosphate buffered medium with 25 % CO and 100 mM formate. The average OD_{600} for these conditions has been determined as 0.61 in Chapter 3.4.

The abrupt cessation of growth during the vitamin supply assessments is elucidated in the subsequent chapter. To replicate and restart the ALE process, the third subculture in chemical defined medium was employed for subculturing (as indicated in Figure 5 and 6, denoted by the blue dashed line "P0"). Following four passages under standard conditions involving 100 mM formate and 25 % CO, this culture was concurrently inoculated into four distinct experimental conditions:

    A. 100 mM formate and 25 % CO with only Ca-pantothenate supplementation.

    B. 100 mM formate and 25 % CO with a complete set of vitamins.

    C. Solely 100 mM formate with full vitamin supplementation, subsequently utilized for continuous bioreactor cultivation.

    D. A positive control condition, which included 2 g L^{-1} yeast extract (YE).

In the first two conditions a strain enhancement indicated by increasing biomass concentration over several passages was observed. The third lineage of subcultures, where formate was exclusively utilized, no visible improvement or enhancement in the observed growth patterns was evident across successive subcultures. Figure 7 illustrates the four parallel lineages subjected to this experimental condition. These established formate subcultures served as the foundation for subsequent inoculation of the bioreactor. This strategic approach ensured the successful transfer of the desired culture into the bioreactor, facilitating continued growth and metabolic activity in a controlled and optimized manner.
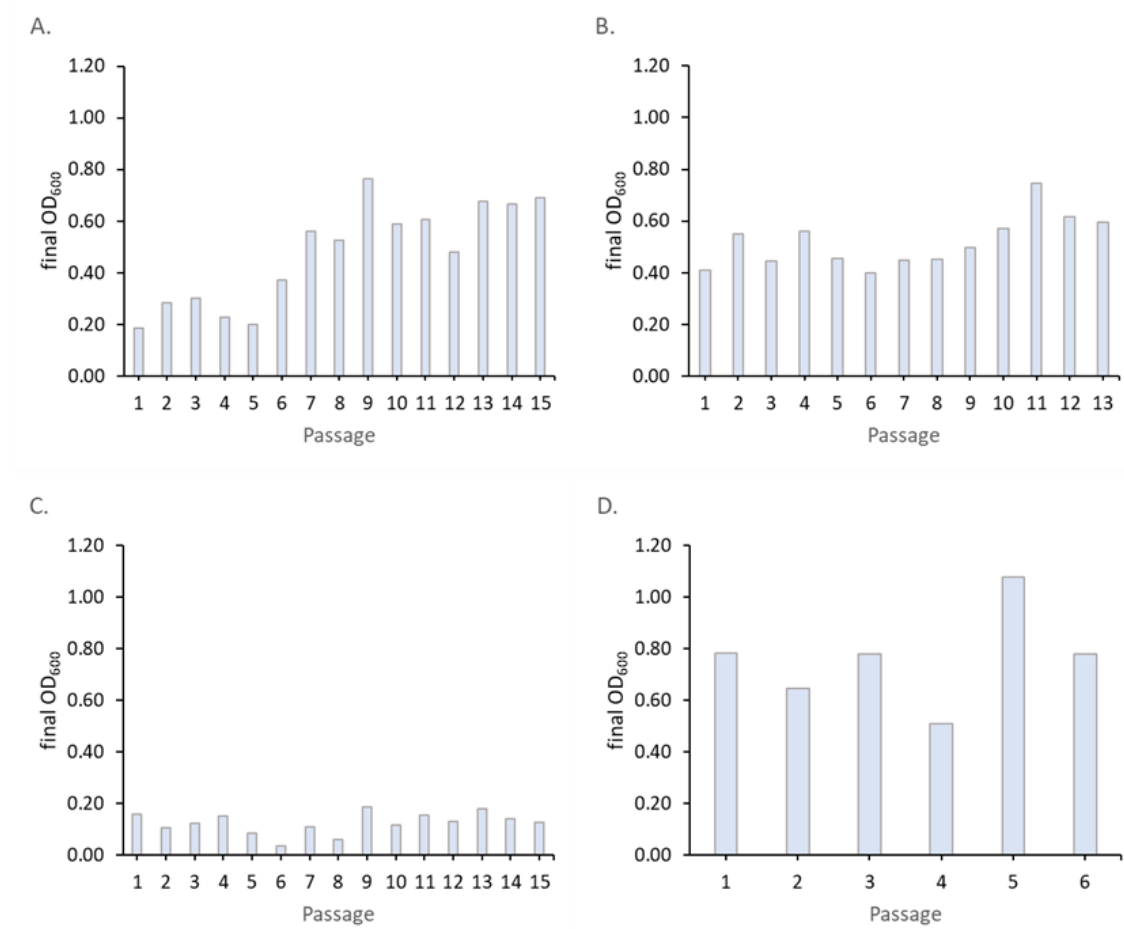
Figure 7: Final optical densities of parallel subcultures under different conditions. **A.** 100 mM formate and 25 % CO with Ca-Pantothenate. **B.** 100 mM formate and 25 % CO with full vitamins. **C.** 100 mM formate with full vitamins. **D.** 100 mM formate and 25 % CO + 2 g L^{-1} YE with full vitamins.

The comparative analysis and discussion of the two distinct vitamin supplementation conditions have been described in detailed in Chapter 3.4 of this study. Notably, a marginal improvement in the final optical density was discerned under both conditions. Specifically, in Condition **C.**, where formate served as the sole substrate, there was an absence of discernible increase in both the final optical density and the growth rate. The mean final OD was found to be 0.143 in this particular condition.

In contrast, the positive control experiment, which utilized yeast extract as a supplement and thereby provided a complex medium, exhibited notably superior growth rates. This observation was attributed to the enhanced availability of nutrients in the complex medium.

3.1.1 Unexpected Growth Cessation

In the second part of the genealogy (Figure 6), it is evident that none of the inoculated subcultures exhibited further growth. In the case of the phosphate buffered medium, this cessation occurred immediately after transitioning from a complete vitamin composition to the inclusion of only one specific vitamin, namely pantothenate. However, it is noteworthy that a control subculture containing only pantothenate and an additional 25 mM fructose displayed robust growth. On the other hand, when observing the right side corresponding to the carbonate buffered medium, growth also ceased after three passages without the full vitamin complement. The pH was examined and found to be within the same range as before. It remained unclear whether the vitamin supply was the limiting factor.

New serum bottles (not shown) were inoculated; however, once again, no growth was observed within 48 hours. Since it seemed unlikely for both media to have deteriorated simultaneously, the carbon sources were considered as a potential issue. A newly prepared anaerobic and sterile formate stock was generated. In addition, all stock solutions, including vitamin stocks, trace elements, carbonate, and phosphate buffer stocks, were systematically renewed. Subsequently, serum bottles were filled and prepared using these newly acquired stock solutions. Finally, the cells were inoculated from a cryo sample from passage 10, resulting in successful growth. Subcultures also exhibited growth.

The primary cause of this problem remains unclear, nonetheless, the hypothesis is that the formate feed stock may have contributed to the problem. In future experiments, it is recommended to conduct parallel comparisons between the previous and desired conditions during passage changes. This approach will facilitate understanding the source of the error.

3.2   Media Selection

The DSM (German Collection of Microorganisms and Cell Cultures) recommends the use of DSMZ 135 medium for *A. woodii*. However, this medium contains a sodium bicarbonate buffer which is unsuitable for the purposes of this study. A Na^+ concentration of 60 mM is desired to optimally support the chemiosmotic mechanism of ATP synthesis (Imkamp & Müller, 2002). The recommended amount of $NaHCO_3$ in the medium corresponds to a Na^+ concentration of 120 mM.

By utilizing a phosphate-buffered medium, this issue could be circumvented. The medium was revised in this laboratory before the onset of this study by Novak et. al. 2021

for *A. woodii* cultivation as well (Novak et al., 2021). This selection ensures a controlled and more favorable environment for the biosynthesis of formate and CO into acetate.

To emphasize the quality of the medium, parallel growth experiments were conducted in serum bottles. The results are graphically presented and will be interpreted subsequently.
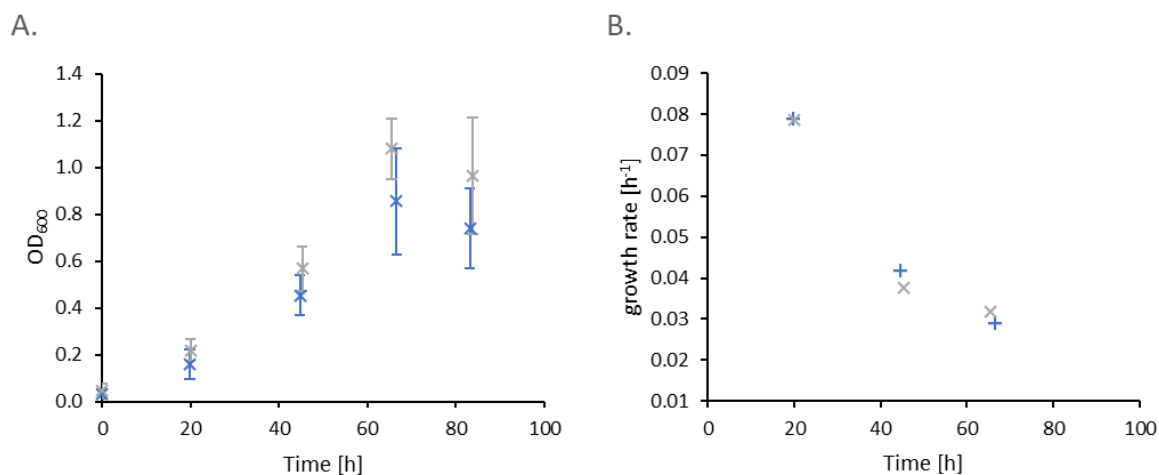
Figure 8: Growth conditions in phosphate buffered (blue crosses) and carbonate buffered (gray crosses) medium. 100 mM formate and 25 % CO is used as carbon source. **A.** Illustration of otiptical density over time. **B.** Illustration of specific growth rate over time. The error bars correspond to the standard deviation and n = 5 for both medium conditions.

Figure 8 presents a comprehensive depiction of the optical density trends and corresponding growth rates over a series of five consecutive passages in both phosphate and carbonate buffered media. The media selection part of the genealogy, as illustrated in Figure 5, delineates the chosen passages, encompassing P6 to P10 for the phosphate medium and P1 to P5 for the carbonate medium. Notably, the mean OD values for the carbonate medium consistently surpass those of the phosphate medium, exhibiting an increase of approximately 25 to 30 % at all measured time points. Nevertheless, it is important to underscore that the presence of relatively high standard deviations, as evidenced by the error bars, precludes the establishment of statistical significance in these findings.

The growth rates were computed based on the mean OD values, and, consequently, standard deviations were not calculable for this metric. The calculations reveal a specific growth rate of 0.08 h^{-1} for both conditions within the initial 20 hours of cultivation. Subsequently, growth rates diminishing by approximately 50 % to 0.04 h^{-1} at the 45-hour mark. A further decline in growth rate is evident at the subsequent measurement point after 63 hours, and after approximately 84 hours, a slight decrease in biomass is observed under both conditions.

Despite the marginal growth advantage observed in the carbonate-buffered medium, the phosphate-buffered medium was the preferred choice due to its intended use in the subsequent bioreactor experiments in this study. A decision was reached to forego the use of carbonate and, instead, to employ a phosphate-buffered medium for all forthcoming experiments and assays.

3.3   Substrate Variations of CO and Formate

Initially, the strain was cultivated using a growth medium containing yeast extract, fructose, and a gas mixture of N_2, H_2, and CO_2. Subsequently, the gas phase was modified by omitting H_2 and CO_2 and introducing formate. In the next stage, fructose was partially replaced by 25 % CO. Following this, yeast extract was completely eliminated, resulting in a chemically defined medium consisting of 100 mM formate and 25 % CO. These passages are illustrated in chapter 3.1, Figure 5. After four passages, the final optical density at 600 nm increased to 0.523. At this point, parallel cultures were inoculated using two different media: carbonate-buffered and phosphate-buffered.

3.3.1 Synergistic Utilization of Formate and CO

After two subcultures in carbonate-buffered medium, modifications were made to the substrate composition. In parallel serum bottle experiments, three different modifications using 100 mM formate with either 25 or 50 % CO and one condition with 25 % CO as the sole substrates were analyzed. Figure 9 depicts the growth profiles over time for the three conditions, which were observed for three passages.

No significant changes were observed over three passages when using 100 mM formate + 25 % CO (Figure 9A) or 100 mM formate + 50 % CO (Figure 9B) as the substrate. Surprisingly, a slightly higher final OD was observed when the CO content in the gas phase was 25 %, even though less carbon was available for growth. Considering that using more than 25 % CO was not advantageous for growth, this concentration was selected for further strain selection.

In the third condition, where carbon monoxide served as the sole carbon and energy source, a minimal increase in biomass was observed during the first passage. However, during the second passage, cell lysis occurred. This observation suggests that there might have been residual formate present in the first passage, leading to limited growth. Subsequent subculturing under these conditions resulted in no observable growth. These results show that *A. woodii* is not capable of using carbon monoxide as the sole carbon and energy source.

A.

B.

C.
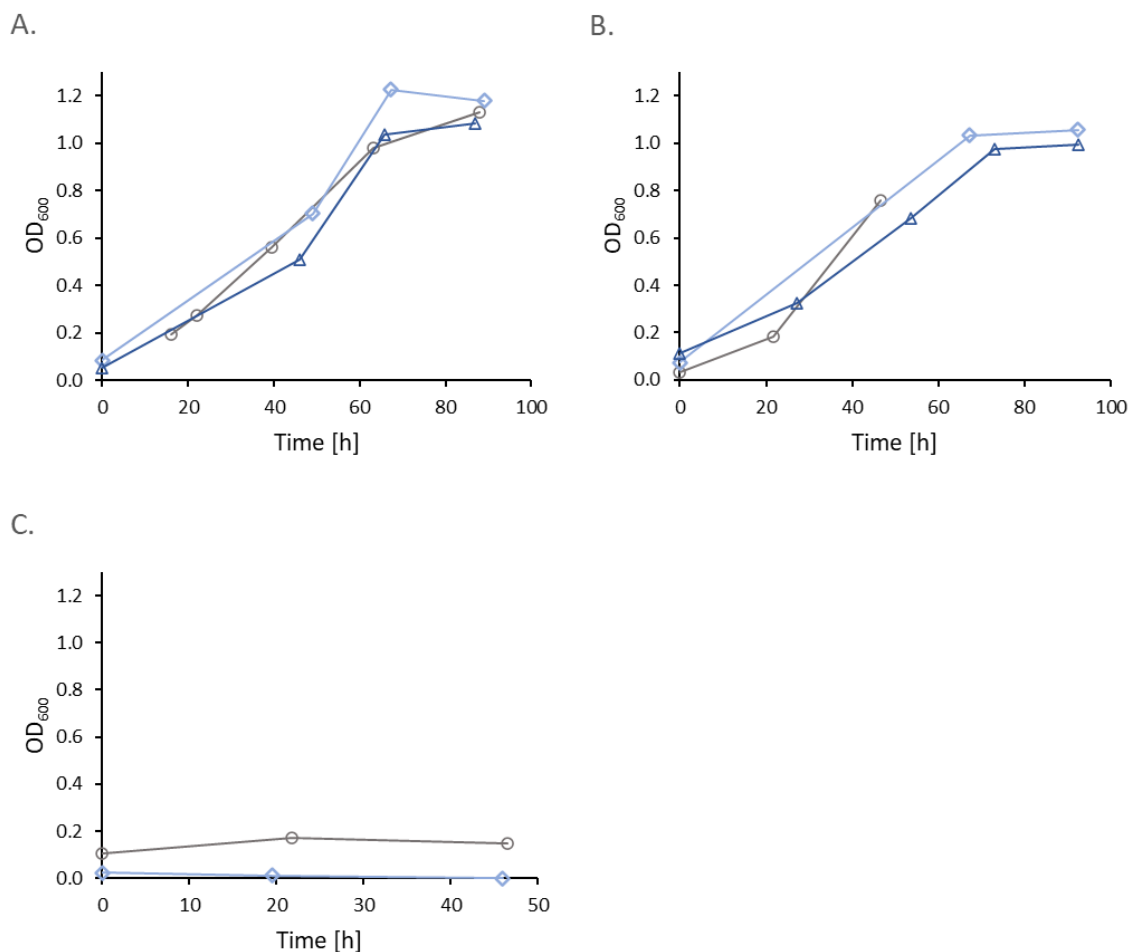
Figure 9: Passages in carbonate buffered medium with different carbon supply. **A.**: 100 mM formate + 25 % CO. **B.**: 100 mM formate + 50 % CO. **C.**: 25 % CO.

Passage 1: ⊖ Passage 2: ◇ Passage 3: △

The observations made in this study regarding the concentration of carbon monoxide in the gas phase provide insights into the metabolic dynamics of *A. woodii*, particularly in the context of its ability to utilize CO as a substrate. One striking finding is that gas-phase CO concentrations exceeding 25 % do not confer any growth advantage, and this can be attributed to the inhibitory effect exerted on two critical hydrogenase enzymes integral to the WLP. The inhibitory effect of CO on these enzymes has been elaborated upon in the introductory section (Chapter 1.5.1).

Furthermore, the inability of *A. woodii* to exhibit growth when supplied with CO as the sole carbon and energy source is a noteworthy result. Prior research has indeed demonstrated that the presence of CO, CO_2, and H_2 can restrict the growth of *A. woodii*. Enzyme studies have revealed that the HDCR complex can utilize Fd^{2-} instead of hydrogen as a reducing equivalent (Schuchmann & Müller, 2013). This Fd^{2-} is generated through the oxidation of CO to CO_2 at the CODH complex. However, it is important to

note that concurrent with this metabolic flexibility, CO exerts inhibitory effects on the HDCR complex, making metabolic activities impossible and consequently leading to a complete absence of growth.

3.3.2 Formate as the sole Carbon and Energy Source

Formate utilization as the sole carbon and energy source was evaluated in serum bottles and selectively enhanced before inoculating the bioreactor.

Under 100 mM formate conditions, a mean OD_{600} of 0.143 with a relative standard deviation of 20 % was observed (Figure 10).

In order to investigate the influence of formate concentration on microbial growth, a stepwise adaptation approach was employed in serum bottles. The initial formate concentration of 100 mM was stepwise increased over five passages until reaching 200 mM. Attempts to directly inoculate from 100 mM to 200 mM formate were unsuccessful, highlighting the need for gradual adaptation. In consideration of the comparison between the resulting final biomass concentration and growth rate under the existing conditions, a further increase in formate concentration was not pursued.

Surprisingly, despite doubling the substrate concentration, a slight decrease in biomass concentration of approximately 13 % was observed. Nevertheless, this deviation is in the range of the standard deviation and therefore statistically not significant. The underlying mechanisms driving this behavior remain unclear. It was anticipated that as the cell population increases, the availability of formate would decrease, thereby reducing any potential inhibitory effects and resulting in higher biomass production. However, the observed trend suggests a more complex relationship between formate concentration and growth.

Figure 10 presents a comparison between the two formate concentration conditions, contrasting the biomass concentration and growth rate. No significant increase of the final biomass concentration and the growth rate was observed over the passages of these two conditions. For 100 mM formate 8 passages have been analyzed to get the mean value and the standard deviation of the final optical density and the growth rate. For 200 mM 6 passages have been analyzed.

A.

B.
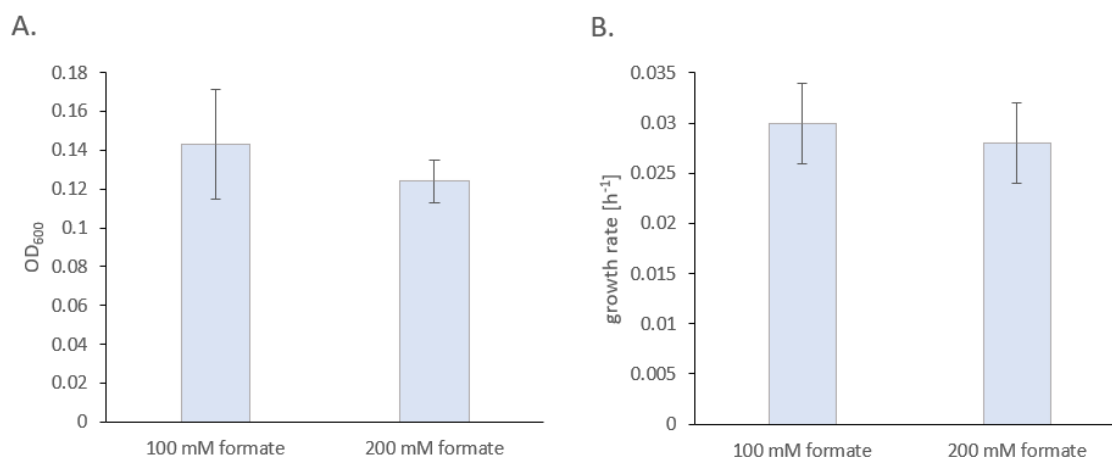
Figure 10: Comparison between 100 (n = 8) and 200 (n = 6) mM formate concentration conditions, contrasting the biomass concentration (**A**) and growth rate (**B**). Conducted in 125 mL serum bottles.

The final biomass concentration occurred between 80 and 100 hours after the introduction of the inoculum, under both experimental conditions. During the initial 20 hours, little or no growth was observed, indicating a lag phase. Following this, the acceleration phase lasted until approximately 35 to 40 hours. Subsequently, the growth phase commenced, characterized by a calculated growth rate μ of around 0.03 h^{-1}, as determined by measuring the optical density at 600 nm. The protracted lag phase and slow acceleration phase can be attributed to metabolic factors. An idealistic logarithmic graph out of the average values of these observations is presented in Figure 11.
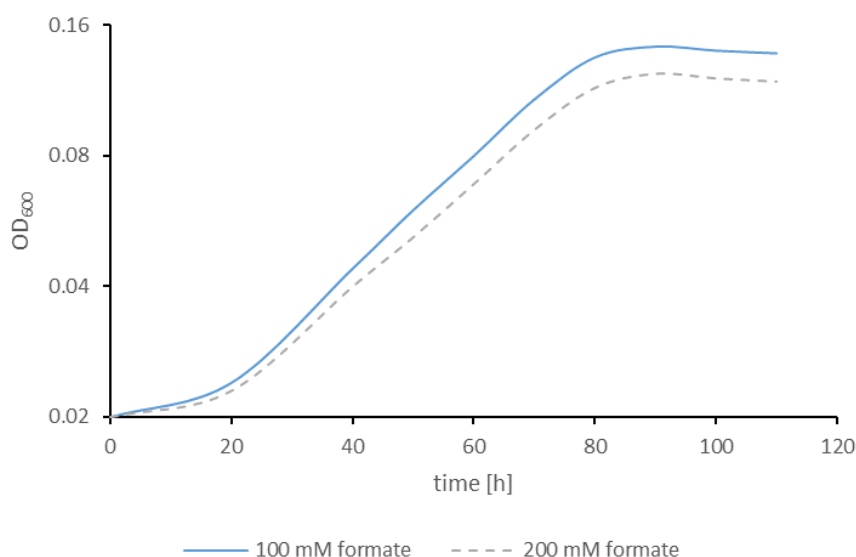
Figure 11: Idealistic biomass concentration over time for two different formate concentrations. The curve representing 100 mM formate and the curve corresponding to 200 mM formate comprise the smoothed mean values derived from all eight and six passages, respectively. The y-axis is presented logarithmic to base 2 to highlight the exponential growth phase.

It is noteworthy that the final OD achieved with formate as the sole carbon source is approximately four times lower than that observed when a substrate mixture of formate and CO is used. *Acetobacterium woodii* is known for its ability to thrive at thermodynamic limits, and this particular growth condition, characterized by formate as the sole carbon source, represents a previously unexplored territory in the context of this organism's metabolic capabilities. To gain a comprehensive understanding of the effects of formate concentration, it is crucial to analyze not only biomass but also substrate and acetate concentrations. These additional measurements will provide valuable insights into the metabolic dynamics and potential limitations imposed by varying formate concentrations.

3.4   The Influence of Vitamins

To validate a finding from a study conducted 46 years ago, experiments were performed using both a full vitamin supply and only Ca-pantothenate (Balch et. al. 1989). The concentration of vitamins used in this study has been increased compared to the recommended levels, as described in the material and method section. Balch et. al. 1989 suggested pantothenate alone could fulfill *A. woodii's* vitamin requirements. The following experiments aimed to validate this finding by comparing full vitamin supply with only Ca-pantothenate. Figure 12 illustrates the final optical densities and specific growth rates under the two different vitamin conditions.

Initially, the final ODs were lower when B_5 was the sole vitamin provided. However, after several passages, no statistically significant difference was observed between the two conditions. The parallel experiment ended with an estimation of the final optical density of 0.64 and 0.61 for Ca-pantothenate and full vitamin conditions, respectively. The specific growth rate was about 0.055 h^{-1} for both conditions. The detailed statistical evaluation is conducted below.
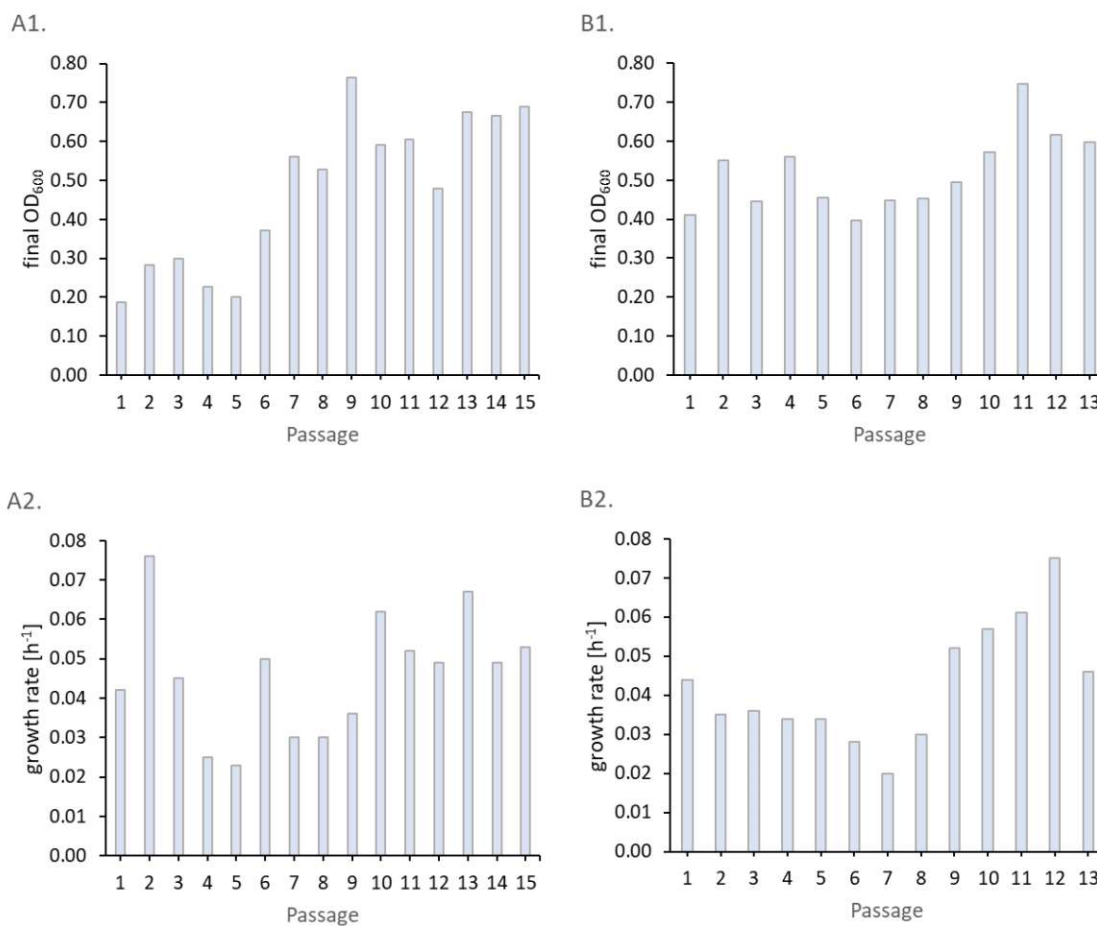
Figure 12: Influence of vitamin supply on final optical density (A1 and B1) and specific growth rate (A2 and B2) over some passages. **A1** and **A2**: 100 mM formate and 25 % CO with Ca-pantothenate in 125 mL serum bottles. **B1.** and **B2.**: 100 mM formate and 25 % CO with full vitamin supply in 125 mL serum bottles.

An unpaired two-tailed t-test was performed to analyze the final OD values obtained from passage 9 onwards. The dataset consisted of two groups: Ca-Pantothenate and full vitamins. The mean values of the final OD for the Ca-pantothenate and full vitamins groups were 0.6400 and 0.6080, respectively, with corresponding standard deviations of 0.0898 and 0.0915. The sample sizes for these groups were 7 and 5, respectively. The statistical analysis yielded a two-tailed p-value of 0.5593. Based on conventional criteria, this p-value indicates that the observed difference between the two groups is not considered to be statistically significant. In other words, the disparity between the means of the Ca-Pantothenate and Full Vitamins groups is not likely to be meaningful from a statistical standpoint.

An unpaired two-tailed t-test was conducted to analyze biomass growth rates as well. The average biomass growth rate was 0.05257 for Ca-Pantothenate and 0.05820 for full vitamins. The standard deviations were 0.00998 and 0.01094. Sample sizes were 7 and 5 for the respective groups. The outcome of the statistical assessment yielded a two-tailed P value amounting to 0.3760. In accordance with established conventions, the two groups

do not exhibit statistical difference. In simpler terms, the variation in growth rates between these groups is likely due to random factors rather than meaningful differences.

The statistical analyses conclude that there exists no noteworthy difference between the cultures supplemented with complete vitamins and those dependent exclusively on Ca-pantothenate. This experimental outcome is in reliance with the study of Balch et. al. 1989.

These experiments demonstrated that *A. woodii* indeed requires only one vitamin, namely pantothenate. Evidently, A. woodii possesses all synthesis pathways to produce all vitamins except for Ca-pantothenate and thus does not require their presence in the growth medium. This finding holds potential significance for industrial applications, as vitamins can be expensive. Consequently, the next step would involve determining the minimum amount of Vitamin B_5 required for a specific cell quantity, which could greatly contribute to cost optimization and process efficiency.

Understanding the minimal vitamin requirements of *A. woodii* not only reveals its metabolic capabilities but also offers insights into potential strategies for industrial-scale production. By identifying the specific vitamin needed and determining the optimal concentration, the overall cost and resource requirements for cultivating *A. woodii* can be optimized, facilitating its potential implementation in industrial settings.

3.5   *Acetate Bioproduction in Continuous Cultures*

Due to the low growth rate observed (approximately 0.03 h^{-1}) when utilizing 100 and 200 mM formate as the sole carbon and energy source, it was considered necessary to initiate the chemostat mode with 200 mM formate and a dilution rate of 0.025 h^{-1}. Consequently, a Pre-Culture derived from the 100 mM formate lineage was prepared and inoculated when it reached an OD_{600} of 0.310 after a period of 4 days. Both the pre-culture medium and the medium employed during the batch phase in the reactor contained 2 g L^{-1} Yeast Extract to facilitate growth. However, it is important to note that this safety measure was solely implemented for the initial reactor startup. Subsequent reactor startups involved a pre-culture without YE (as well from the 100 mM formate lineage), and only a minimal amount (0.5 g L^{-1}) of YE was initially added to the reactor. All feed media were prepared without YE. Post start-up, at least four volume changes were performed before calculating the steady state to ensure the complete removal of YE from the reactor system. Once achieving steady state conditions for a minimum of two volume changes, the dilution rate, or the concentration of formate in the feed were continuously altered. In cases where cells were washed out or steady chemostat conditions were unattainable, the reactors underwent autoclaving, cleanup, and preparation for new inoculation.

The following sections will delve into the reached steady states, their calculations, and the resulting outcomes compared to the results of the study from Neuendorf et. al. 2021, followed by a discussion of the observations and challenges encountered during the cultivation of A. woodii in the bioreactor. Steady States of Continuous Bioproduction of Acetate

This chapter presents a thorough exploration of steady state dynamics during continuous acetate bioproduction through *A. woodii*. In bioproduction processes, the establishment and maintenance of steady states are pivotal for both understanding microbial behavior and optimizing desired outputs. Specifically, the impact of varying formate concentrations and dilution rates on the attainment of these steady states and a comparison between the study of Neuendorfer et. al. has been investigated (Neuendorf et al., 2021).

The experimental design involved maintaining each established steady state for a minimum of 2 volume changes before transitioning to the subsequent condition. Commencing at a dilution rate of 0.025 h^{-1} and a formate concentration of 200 mM, the study ended at a dilution rate of 0.2 h^{-1} and a formate concentration of 300 mM. Attempts to maintain stability with a formate concentration of 500 mM, as detailed in the upcoming Chapter (3.5.2), turned out to be a failure. The implementation of a gradual transition to this concentration in further exploration could led to positive results.

Central to our analysis is Table 4, which comprehensively outlines acetate and biomass concentrations, formate consumption-related yields, volumetric and specific rates, carbon balance, and degree of reduction at different dilution rates, with a uniform feed concentration of 200 mM formate throughout. Of note, the last entry in this table draws from a parallel study by Neundorf et al., differing primarily in the application of YE (2 g L^{-1}) during the entire fermentation process whereas a chemical defined medium was applied for this study.

Analogous constructed to Table 4, Table 5 has a uniform feed concentration of 300 mM formate, elucidating the impact of altered conditions on the steady state parameters.

3.5.1 Volumetric Rates at 200 mM Formate Feed Concentration

When comparing the volumetric rates across the replicates conducted under 200 mM formate concentration, a striking consistency and proximity among the results become evident. The depiction of these volumetric rates in relation to the corresponding dilution rates reveals a noticeable upward trend across all parameters. This observation is not only confined to the rates observed in this investigation; rather, it resonates harmoniously with the volumetric rates documented in the study by Neuendorf et. al. (Neuendorf et al., 2021). The alignment of these rates is further illustrated in Figure 13, in which a linear correlation with the dilution rate was assumed. The associated equations for this

correlation are presented below, accompanied by the corresponding coefficients of determination (R^2). Under the prevailing 200 mM formate concentration, the maximum feasible dilution rate remains unattained, thereby offering prospects for further exploration.
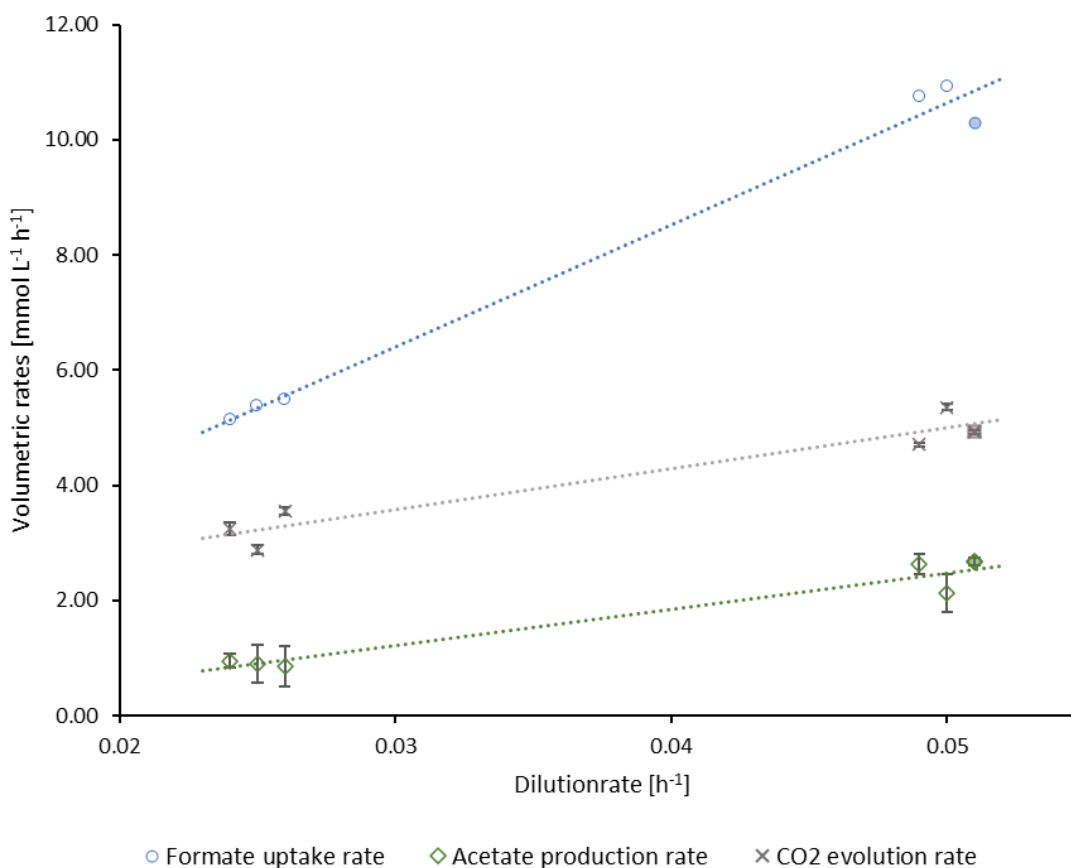
Figure 13: Steady states of the volumetric rates corresponding to dilution rates in a continuous process with 200 mM formate feed concentration. Each data point corresponds to a minimum of two measurements, and its standard deviation. The filled points at a dilution rate of 0.05 h^{-1} have been taken from Neuendorfer et. al., 2021.

Equation 17: An empirical correlation emerges between the dilution rate and the volumetric formate uptake rate, evident under a constant formate feed concentration of 200 mM.

$$r_{For} = 211.9 \cdot D + 0.053$$

$$R^2 = 0.9883$$

Equation 18: An empirical correlation emerges between the dilution rate and the volumetric acetate production rate, evident under a constant formate feed concentration of 200 mM.

$$r_{Ace} = 62.51 \cdot D - 0.656$$

$$R^2 = 0.9461$$

Equation 19: An empirical correlation emerges between the dilution rate and the volumetric CO_2 evolution rate, evident under a constant formate feed concentration of 200 mM.

$$r_{CO_2} = 70.99 \cdot D + 1.446$$

$$R^2 = 0.9238$$

All volumetric rates are expressed in mmol L^{-1} h^{-1}, while all dilution rates are denoted in h^{-1}.

At a dilution rate of 0.025 h^{-1}, the volumetric acetate production rate (r_{Ace}) was measured at approximately 0.90 mmol h^{-1} L^{-1}, while the volumetric CO_2 evolution rate (r_{CO2}) was found to be approximately 3.22 mmol h^{-1} L^{-1}. Doubling the dilution rate to 0.05 h^{-1} resulted in an increase in r_{Ace} to approximately 2.37 mmol h^{-1} L^{-1} and r_{CO2} to approximately 5.02 mmol h^{-1} L^{-1}. This twofold increase in the dilution rate to 0.05 h^{-1} led to an increase factor in acetate production and CO_2 evolution rate of 2.63 and 1.56, respectively. Consequently, it is postulated that higher dilution rates are more efficient for the conversion of formate to acetate under the observed conditions. This observation is further elucidated through yield calculations in the subsequent section.

A direct comparison with the data from the study conducted by Neuendorfer et al. in 2021, at a dilution rate of 0.05 h^{-1}, revealed slightly higher volumetric acetate production rates and slightly lower volumetric CO_2 evolution rates. In this study, the rAce was approximately 2.37 mmol h^{-1} L^{-1}, whereas in the comparison study, the value was 2.67 mmol h^{-1} L^{-1}. It is worth noting that the standard deviations of these mean values allowed for some overlap between the ranges. Another potential factor contributing to the higher volumetric acetate production rate in the comparison study is the conversion of certain components within the yeast extract used. The possibility of a partial conversion of components within the yeast extract could potentially account for the observed higher acetate yields than what is stoichiometrically predicted. This matter will be examined in more detail in the upcoming section (Neuendorf et al., 2021).

While the experiment was restricted to a dilution rate of 0.05 h^{-1}, it is conjectured that a dilution rate of 0.1 h^{-1} is attainable. This determination was driven by the observation of specific growth rate values of 0.087 and 0.331 h^{-1} during the prior batch phase (Chapter 3.5.7.3). Additional reason for this projection comes from subsequent observations conducted under a formate concentration of 300 mM, where a dilution rate of 0.1 h^{-1} was successfully achieved without the formation of a biofilm.

3.5.2 Specific Rates at 200 mM Formate Feed Concentration

The specific rates are presented graphically in Figure 14 as a function of the dilution rate. Notably, the measured biomass concentration exhibits significant variability across independent steady states conducted under identical conditions. Furthermore, the biomass

concentration is not consistently stable within each steady state, as evidenced by the presence of error bars. In essence, there appears to be no discernible correlation between the biomass concentration and the examined dilution rates of 0.025 and 0.05 h^{-1} under a 200 mM formate feed. Consequently, the experimental results do not yield any specific rates that can be reliably determined.

Figure 14: Steady states of the specific rates corresponding to dilution rates in a continuous bioreactor process with 200 mM formate feed concentration. Each data point corresponds to a minimum of two measurements, and its standard deviation.

While acknowledging the inherent variability within biological and biochemical systems, it is noteworthy that the biomass concentration exhibits a pronounced degree of variability under the observed dilution rates and a concentration of 200 mM formate. This variance may stem from the adaptability of cells within a broad substrate availability range, when the dilution rate remains far below their maximal growth rate within the given conditions. Alternatively, this variance might be attributed to an unnoticed biofilm forming within the reactor, causing measurements of reactor liquid samples inadequate in accounting for cells adhering to surfaces like reactor walls, stirrer blades, or baffles.

3.5.3 Yields, Carbon Balance, and Degree of Reduction at 200 mM Formate Feed Concentration

The acetate yields exhibit substantial variability, primarily attributed to fluctuations in acetate concentration at the measurement points during steady states. Furthermore, independent steady states yield different acetate yields as well. Figure 15 provides a visual representation of the acetate yields under various conditions.
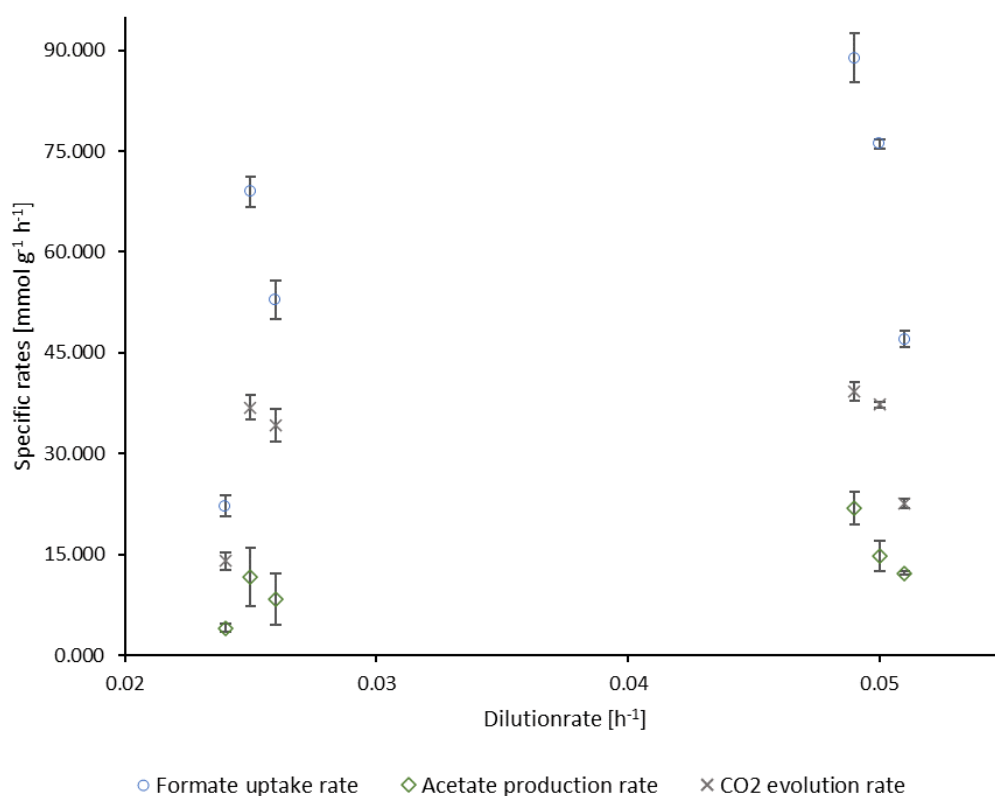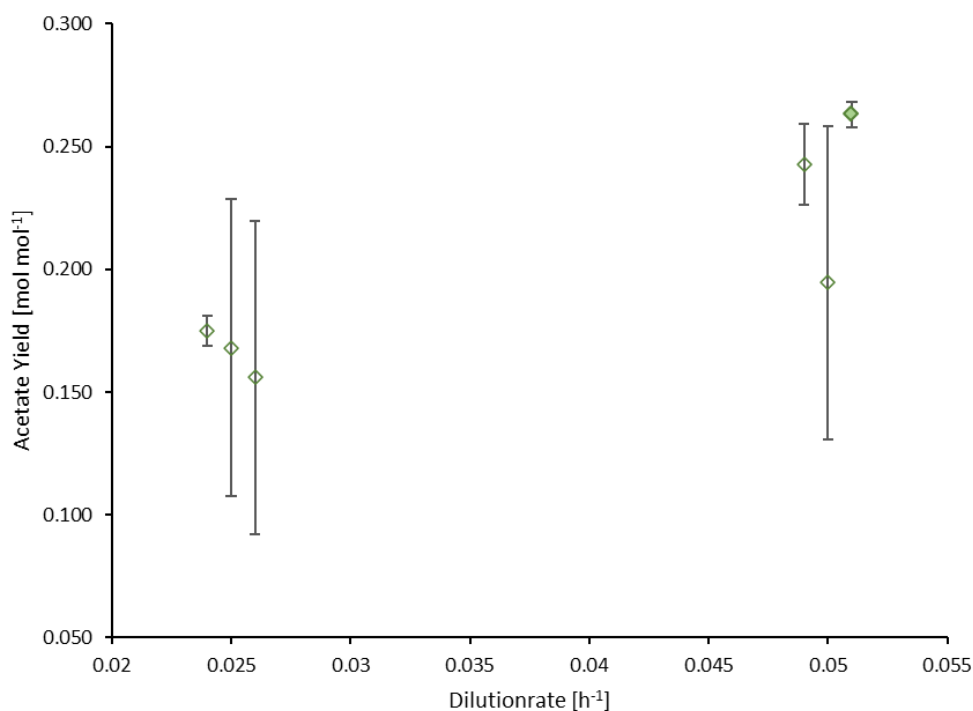

Figure 15: Comparison of acetate yields corresponding to dilution rates in a continuous bioreactor process with 200 mM formate feed concentration. Each data point corresponds to a minimum of two measurements, and its standard deviation.

Despite this inherent and pronounced variability, it is hypothesized that higher dilution rates result in higher acetate yields. In the comparative study conducted by Neuendorfer et al. in 2021, the yield was calculated to be 0.263 ± 0.005 when a dilution rate of 0.05 h^{-1} was maintained. As mentioned previously, the maximum stoichiometric yield achievable through the conversion of formate to acetate is 0.250, which theoretically represents the upper limit. It is plausible that the conversion of certain components within the yeast extract used in the comparative study may have contributed to this higher yield.

The variability in yield primarily stems from varying biomass concentrations, which in turn affect acetate production, rendering the overall system variable. Nonetheless, the acetate yield at a dilution rate of 0.05 h^{-1} is not believed to significantly deviate from the theoretically possible value of 0.250. The Carbon Balance demonstrates a high level of accuracy across the entirety of the tested conditions, as evidenced by its proximity to the

theoretical value of 100 %. (Table 4). This alignment underscores the correctness of the measurements and evaluation methodologies.

In contrast, the Degree of Reduction Balance exhibited a discrepancy in closure, notably in the case of R11-F2, with a value of 166 % and an exceptionally high standard deviation. One contributing factor to the elevated degree of reduction values pertains to the progressive decline in biomass concentration during the corresponding period. Moreover, the dynamic behavior of acetate concentration exhibited an initial decrease followed by subsequent increments and subsequent decline (Attachment, Figure 22). This fluctuation generate variability in the calculated rates, thereby introducing imprecision into the degree of reduction determinations. For all hydrogen measurements conducted in reactor 11 (R11) had signal inaccuracies. All measurements are precluded and not displayed in this work. It is postulated that the H_2 rates are of low magnitude, and consequently, their influence on the degree of reduction value is minimal. Nonetheless, this phenomenon contributes to a systematic error, even if of minor significance.

3.5.4 Volumetric Rates at 300 mM Formate Feed Concentration

After studying continuous reactor experiments under the 200 mM formate feed flow, the concentration was elevated towards 300 mM. This elevation in formate concentration led to expected higher volumetric rates, a maximum acetate yield measured at a dilution rate of 0.1 h^{-1}, and the absence of weaknesses at dilution rates as high as 0.2 h^{-1}, likely attributable to biofilm evolution in the reactor.

Figure 16 illustrates the volumetric rates of formate, acetate, and CO_2. The precision of the linear regression applied to formate and acetate data is notably remarkable. Hence, standard deviations are not depicted as their magnitude is smaller than the symbol displayed for each data point. In the case of CO_2, the regression is based on the initial four steady states, up until a dilution rate of 0.1 h^{-1}, owing to the presence of a measurement drift in the CO_2 sensor. This is derived from the desire to ensure the accuracy of the relationship.

Figure 16: Steady states of the volumetric rates corresponding to dilution rates in a continuous bioreactor process with 300 mM formate feed concentration. Error bars have been omitted from the presentation due to their magnitude being smaller than the symbols representing each measurement point. Each data point corresponds to a minimum of two measurements.

The linear equations for the volumetric rates under 300 mM formate are provided below.

Equation 20: An empirical correlation emerges between the dilution rate and the volumetric formate uptake rate, evident under a constant formate feed concentration of 300 mM.

$$r_{For} = 306.84 \cdot D + 0.325$$

$$R^2 = 0.9999$$

Equation 21: An empirical correlation emerges between the dilution rate and the volumetric acetate production rate, evident under a constant formate feed concentration of 300 mM.

$$r_{Ace} = 65.31 \cdot D - 0.048$$

$$R^2 = 0.9936$$

Equation 22: An empirical correlation emerges between the dilution rate and the volumetric CO_2 evolution rate, evident under a constant formate feed concentration of 300 mM.

$$r_{CO_2} = 84.277 \cdot D + 2.661$$

$$R^2 = 0.9803$$

All volumetric rates are expressed in mmol L^{-1} h^{-1}, while all dilution rates are denoted in h^{-1}. The derived linear equations, while serving as valuable approximations, remaining valid solely within the examined. One of these approximations relies on the assumption of constant product concentrations. However, the observations elucidated in Table 6 show variable concentrations, wherein the acetate concentration displays a subtle upward trend, eventually culminating in a maximum at a dilution rate of 0.1 h^{-1}. In the context of the linear model, the acetate concentration is extrapolated to be 3.85 g L^{-1}. It's important to highlight that in practical scenarios where the acetate concentration reaches its highest point, there naturally must be an ideal acetate yield (Figure 18) associated with this occurrence.

At a dilution rate of 0.05 h^{-1}, the volumetric acetate production rate was measured at approximately 3.11 mmol h^{-1} L^{-1}, and the volumetric CO_2 evolution rate was found to be approximately 7.07 mmol h^{-1} L^{-1}. An increase of the dilution rate to 0.10 h^{-1}, there was an increase in r_{Ace} to approximately 6.94 mmol h^{-1} L^{-1}, and r_{CO2} to approximately 10.73 mmol h^{-1} L^{-1}. This twofold increase of D to 0.10 h^{-1} resulted in an increase factor in acetate production and CO_2 evolution rate of 2.23 and 1.52, respectively. Consequently, it can be inferred that the conversion of formate to acetate is more efficient at a dilution rate of 0.10 h^{-1} as compared to 0.05 h^{-1}.

3.5.5 Specific Rates at 300 mM Formate Feed Concentration

The specific rates are illustrated graphically in Figure 17 as a function of the dilution rate. As the dilution rate increases from 0.025 to 0.10 h^{-1}, the biomass concentration also exhibits an increase. Subsequently, the biomass concentration decreases, simultaneously with the emergence of a biofilm that renders biomass determination unfeasible. Hence, the specific rates at 0.15 and 0.20 h^{-1} are not representable.

Throughout all measurements, there was almost no formate detected within the reactor volume, suggesting complete substrate conversion.

It is anticipated that, as the dilution rate approaches the maximum growth rate (μ_{max}) of the cells, the biomass concentration should either remain constant or decrease due to washout. However, this trend was not observed until a dilution rate of 0.1 h^{-1}. Beyond this point, the appearance of a biofilm makes it challenging to discover the maximum growth rate accurately. Therefore, there is a belief that the dilution rate could be increased beyond 0.1 h^{-1}, even in the absence of biofilm formation. However, the exact level to which it can be elevated remains uncertain. Additionally, aside from adjusting the dilution rate, increasing the formate concentration is also a plausible option, as the microorganisms appear robust in terms of complete formate conversion capabilities.
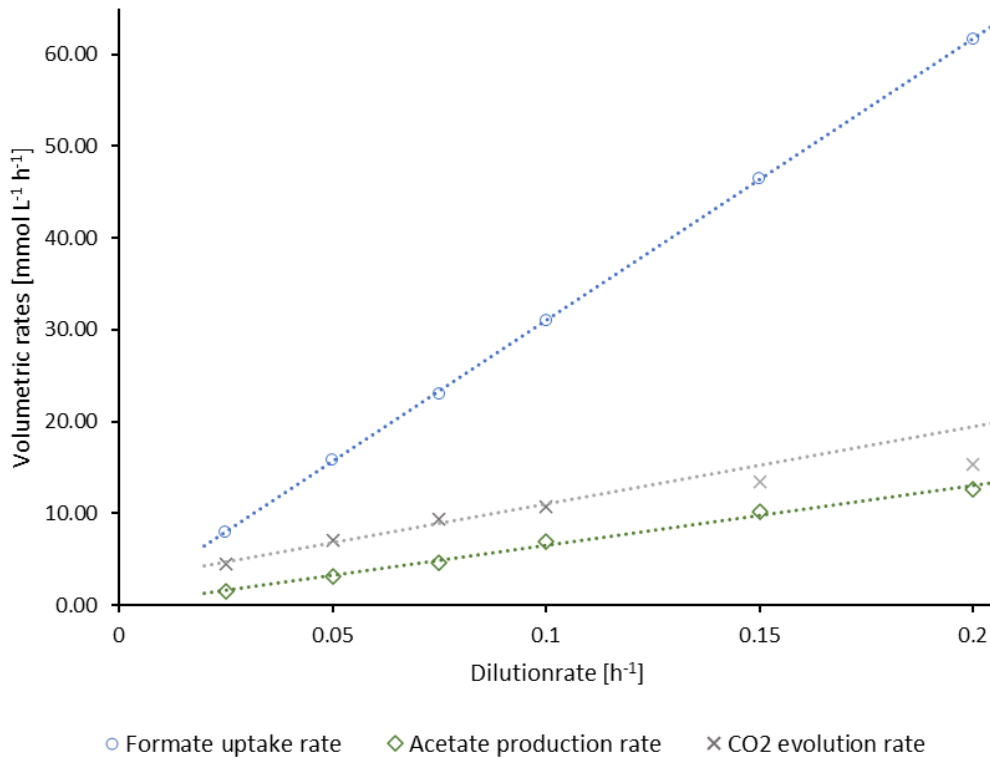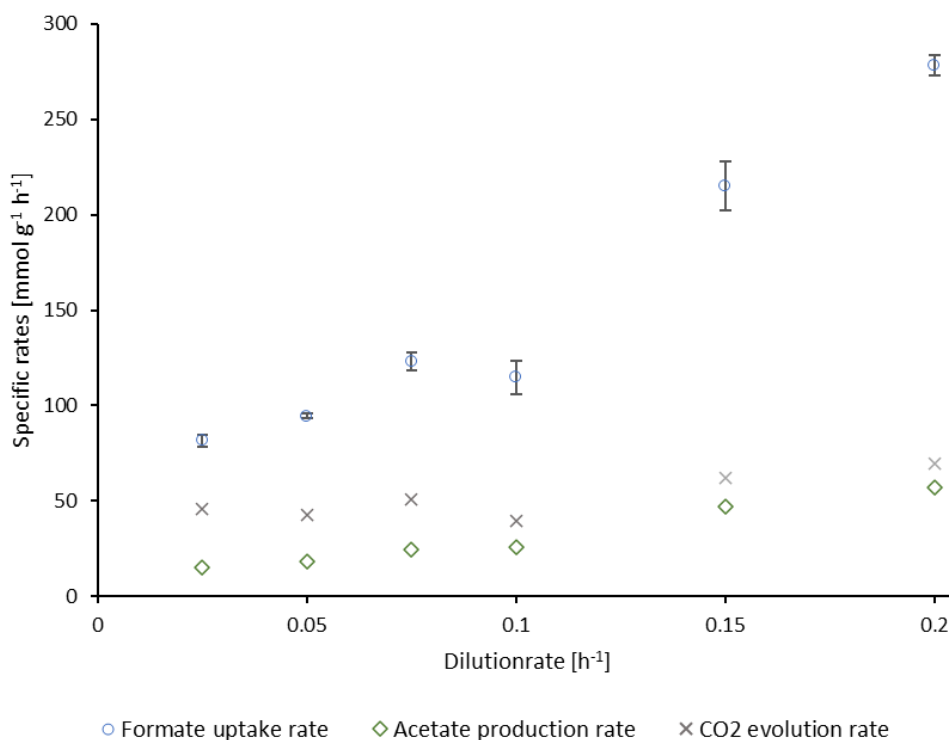
Figure 17: Steady states of the specific rates corresponding to dilution rates in a continuous bioreactor process with 300 mM formate feed concentration. Each data point corresponds to a minimum of two measurements, and its standard deviation.

3.5.6 Yields, Carbon Balance, and Degree of Reduction at 300 mM Formate Feed Concentration

The acetate yield is a parameter quantifying the scope to which formate is utilized for acetate synthesis. The theoretical chemical reachable yield would be 0.250 mol mol h^{-1}, as described in the Chapter 1.5. 1 and 2.5. Figure 18 illustrates the acetate yields associated with the applied dilution rates. At dilution rates of 0.1 h^{-1} and 0.15 h^{-1}, the acetate yields are 0.225 ± 0.002 mol mol^{-1} and 0.218 ± 0.018 mol mol^{-1}, respectively. Despite the considerable standard deviations, the data indicates that the maximum acetate yield falls within the dilution rate range of 0.1 to 0.15 h^{-1} when the feed contains 300 mM formate. Under the condition of a 200 mM formate feed flow, the yields are situated within a comparable range, slightly diminished. However, the presence of high standard deviations precludes precise interpretation. Hence, to establish a more definitive understanding, it is recommended to conduct further experiments under analogous conditions.
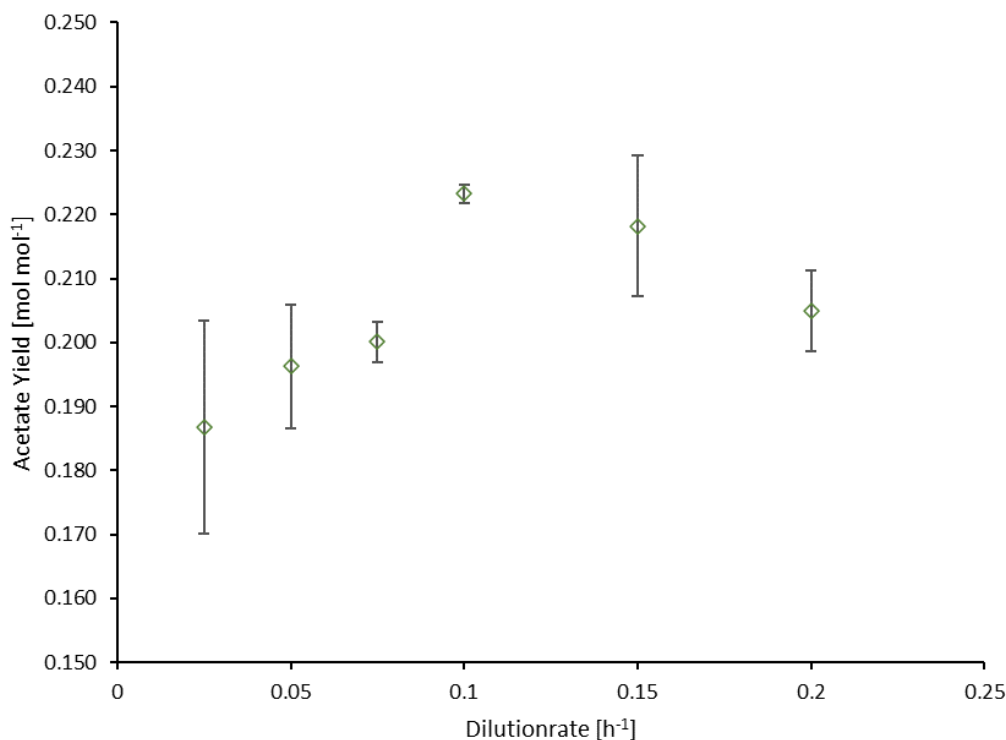
Figure 18: Steady states in a continuous bioreactor with 300 mM formate feed and varying dilution rates. Comparison of acetate Yields under varying dilution rates.

In the context of 300 mM formate and a dilution rate of 0.1 h^{-1} and higher, it is noteworthy to highlight the visibility of a biofilm within the reactor (Chapter 3.5.7.5). This makes the interpretation and comparison of specific rates impractical due to the evident influence of the biofilm. While specific rates are presented in both Table 4 and Table 5, the considerable deviations underscore their limited representativeness.

It is noteworthy that the carbon balance deviates increasingly from its true value of 100 % as the dilution rate rises. This trend suggests a scenario where higher dilution rates result in an implausible outcome—carbon input surpassing carbon output. Such an observation contradicts the principles of mass conservation, as the sum of C-molar yields for biomass, acetate, and CO_2 should theoretically be 1. The stacked bar graph in Figure 19 illustrates these C-molar yields for each dilution rate.

At a low dilution rate of 0.025 h^{-1}, the theoretical yield of 1 is almost reached. However, beyond this point, the sum of yields decreases with increasing dilution rates. It is postulated that the primary source of error lies in inadequate CO_2 measurement. Although the presence of the biofilm also contributes to a reduction in biomass yield, it does not exhibit the same magnitude of impact as observed in the CO_2 yield.
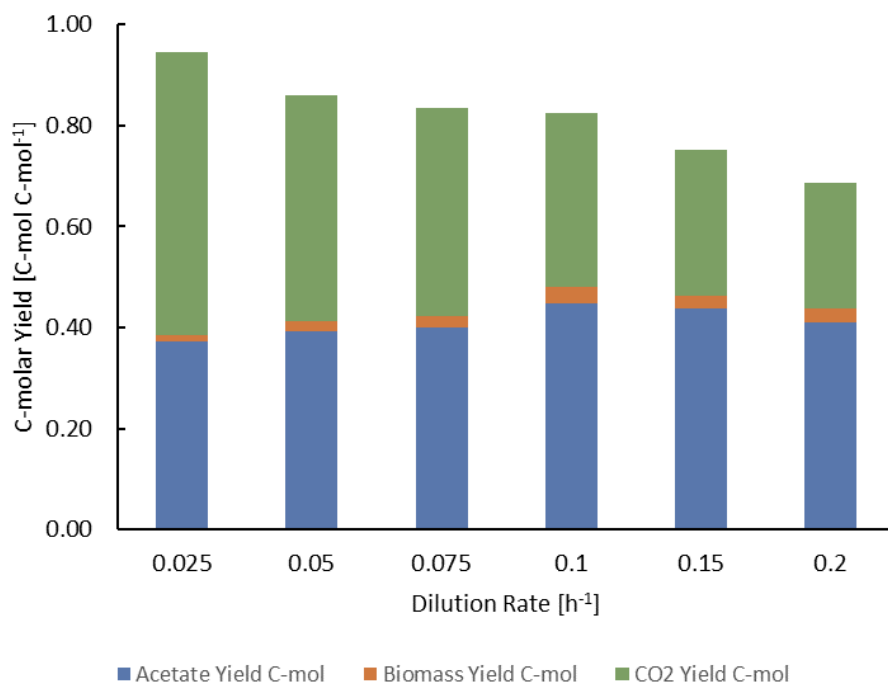
Figure 19: C-molar yields at different dilution rates at 300 mM formate feed flow.

The calculation of C-molar yields involving volumetric formate, acetate, biomass, and CO_2 rates.

The precision of the HPLC measurements for acetate and formate is deemed high, and consequently, it is unlikely to introduce errors in the calculation of yields. The accumulation of biomass, particularly as a biofilm at dilution rates higher than $0.1 \ h^{-1}$, introduces uncertainty as it acts as a carbon sink, potentially contributing to the carbon balance and yield deviation. However, the lower magnitude of biomass rates, compared to other rates, make them less likely to be the primary cause of the imbalance.

As a result, the decline in the cumulative C-molar yields is attributed primarily to inaccuracies in representing CO_2 content by the Blue Sense Sensor. This may be due to sensor calibration drift over the extended process timeline. Therefore, it is suggested to use a Gas Chromatography (GC) for more accurate measurements.

The inaccuracy in carbon dioxide measurements is also reflected in the relationship between carbon evolution rates and dilution rates, particularly at higher dilution rates, leading to the exclusion of certain data points at dilution rates of 0.15 and $0.2 \ h^{-1}$ from the linear correlation analysis (Figure 16). In conclusion, the primary cause of the carbon balance disparity is attributed to inaccuracies in CO_2 measurements, while the influence of volumetric biomass rates is considered secondary due to their lower rates compared to CO_2 rates.

Substrate Concentration 200 mM formate

#	D [h^{-1}]	Concentrations		Yields			Balances	
		Biomass [g L^{-1}]	Acetate [g L^{-1}]	$Y_{X/For}$ [g mol^{-1}]	$Y_{CO2/For}$ [mol mol^{-1}]	$Y_{Ace/For}$ [mol mol^{-1}]	C [out in^{-1}]	DoR [out in^{-1}]
R8-F1	0.025	0.233 ± 0.016	2.156 ± 0.128	1.100 ± 0.155	0.630 ± 0.029	0.175 ± 0.006	103.955 ± 5.211	103.961 ± 9.000
R8-F2	0.025	0.078 ± 0.002	1.965 ± 0.201	0.316 ± 0.113	0.535 ± 0.010	0.168 ± 0.060	88.284 ± 13.202	109.527 ± 25.618
R11-F2	0.025	0.104 ± 0.006	1.861 ± 0.218	0.438 ± 0.085	0.648 ± 0.013	0.156 ± 0.064	97.564 ± 13.378	65.799 ± 24.919
R8-F3	0.05	0.121 ± 0.004	2.756 ± 0.099	0.567 ± 0.053	0.435 ± 0.004	0.243 ± 0.016	94.077 ± 2.667	88.908 ± 4.545
R11-F3	0.05	0.144 ± 0.001	2.475 ± 0.130	0.675 ± 0.040	0.490 ± 0.007	0.195 ± 0.064	89.562 ± 6.201	83.087 ± 12.292
Neuendorf et. al. (2021)	0.05	0.220 ± 0.000	3.170 ± 0.050	1.090 ± 0.030	0.478 ± 0.011	0.263 ± 0.005	104.000 ± 1.000	113.000 ± 0.000

#	D [h^{-1}]	Volumetric rates				Specific rates			
		r_{Ace} [mmol L^{-1} h^{-1}]	r_{For} [mmol L^{-1} h^{-1}]	r_{CO2} [mmol L^{-1} h^{-1}]	r_{H2} [mmol L^{-1} h^{-1}]	q_{Ace} [mmol g^{-1} h^{-1}]	q_{For} [mmol g^{-1} h^{-1}]	q_{CO2} [mmol g^{-1} h^{-1}]	q_{H2} [mmol g^{-1} h^{-1}]
R8-F1	0.025	0.946 ± 0.118	5.145 ± 0.004	3.242 ± 0.104	3.276 ± 1.329	4.085 ± 0.589	22.200 ± 1.545	14.003 ± 1.265	3.276 ± 1.329
R8-F2	0.025	0.906 ± 0.330	5.383 ± 0.036	2.879 ± 0.073	17.316 ± 9.287	11.629 ± 4.370	68.946 ± 2.316	36.884 ± 1.788	17.316 ± 9.287
R11-F2	0.025	0.856 ± 0.351	5.485 ± 0.009	3.552 ± 0.069	-	8.353 ± 3.834	52.810 ± 2.842	34.220 ± 2.396	-
R8-F3	0.05	2.625 ± 0.177	10.762 ± 0.102	4.704 ± 0.038	10.162 ± 0.210	21.938 ± 2.440	88.875 ± 3.713	39.242 ± 1.404	10.162 ± 0.210
R11-F3	0.05	2.124 ± 0.321	10.920 ± 0.062	5.353 ± 0.055	-	14.792 ± 2.233	76.042 ± 0.772	37.279 ± 0.421	-
Neuendorf et. al. (2021)	0.05	2.670 ± 0.060	10.300 ± 0.100	4.920 ± 0.030	0.000 ± 0.000	12.200 ± 0.300	47.000 ± 1.200	22.500 ± 0.700	0.000 ± 0.000

Table 4: Steady States with 200 mM formate feed concentration at various dilution rates.

Substrate Concentration 300 mM formate

#	D [h^{-1}]	Concentrations		Yields			Balances	
		Biomass [g L^{-1}]	Acetate [g L^{-1}]	$Y_{X/For}$ [g mol^{-1}]	$Y_{CO2/For}$ [mol mol^{-1}]	$Y_{Ace/For}$ [mol mol^{-1}]	C [out in^{-1}]	DoR [out in^{-1}]
R11-F4	0.025	0.099 ± 0.003	3.194 ± 0.186	0.290 ± 0.043	0.560 ± 0.006	0.187 ± 0.017	94.146 ± 3.976	76.950 ± 6.993
R11-F5	0.050	0.165 ± 0.005	3.665 ± 0.065	0.562 ± 0.018	0.447 ± 0.000	0.196 ± 0.010	83.589 ± 2.301	82.875 ± 4.001
R11-F6	0.075	0.187 ± 0.005	3.599 ± 0.024	0.610 ± 0.022	0.411 ± 0.008	0.200 ± 0.003	77.632 ± 0.372	84.791 ± 1.432
R11-F7	0.100	0.272 ± 0.020	4.095 ± 0.002	0.875 ± 0.064	0.345 ± 0.002	0.223 ± 0.002	79.597 ± 0.555	96.094 ± 1.086
R11-F8	0.150	0.216 ± 0.013	3.973 ± 0.169	0.698 ± 0.041	0.290 ± 0.014	0.218 ± 0.011	71.870 ± 2.452	92.714 ± 4.682
R11-F9	0.200	0.221 ± 0.003	3.771 ± 0.077	0.718 ± 0.014	0.249 ± 0.025	0.205 ± 0.006	64.694 ± 0.570	87.549 ± 2.423

#	D [h^{-1}]	Volumetric rates				Specific rates			
		r_{Ace} [mmol L^{-1} h^{-1}]	r_{For} [mmol L^{-1} h^{-1}]	r_{CO2} [mmol L^{-1} h^{-1}]	r_{H2} [mmol L^{-1} h^{-1}]	q_{Ace} [mmol g^{-1} h^{-1}]	q_{For} [mmol g^{-1} h^{-1}]	q_{CO2} [mmol g^{-1} h^{-1}]	q_{H2} [mmol g^{-1} h^{-1}]
R11-F4	0.025	1.498 ± 0.142	8.022 ± 0.046	4.491 ± 0.024	-	15.231 ± 0.766	81.704 ± 3.182	45.749 ± 2.281	-
R11-F5	0.050	3.111 ± 0.158	15.854 ± 0.027	7.068 ± 0.034	-	18.548 ± 0.702	94.538 ± 1.076	42.822 ± 1.032	-
R11-F6	0.075	4.584 ± 0.046	22.984 ± 0.251	9.429 ± 0.100	-	24.603 ± 0.547	122.996 ± 4.538	50.575 ± 1.114	-
R11-F7	0.100	6.936 ± 0.049	31.073 ± 0.081	10.727 ± 0.041	-	25.589 ± 1.762	114.677 ± 8.588	39.597 ± 3.164	-
R11-F8	0.150	10.135 ± 0.514	46.446 ± 0.016	13.447 ± 0.661	-	46.885 ± 1.283	215.257 ± 12.725	62.296 ± 4.346	-
R11-F9	0.200	12.637 ± 0.446	61.669 ± 0.271	15.370 ± 1.498	-	57.073 ± 2.859	278.462 ± 5.356	69.351 ± 5.732	-

Table 5: Steady States with 300 mM formate feed concentration at various dilution rates.

3.5.7 Observations and Challenges of the Cultivation in Bioreactor

As previously mentioned, the first bioreactor experiment involved the use of 2 g L^{-1} YE in both the pre-culture medium and the bioreactor medium. To ensure complete washout of YE and eliminate any potential influence on steady-state conditions, four volume changes were implemented after the reactor start-up before initiating the balance period for calculation. In all other bioreactor cultivations YE supplementation was waived in the Pre-Cultures successfully. Nevertheless, to support biomass growth and formate uptake rate in subsequent batch reactors, a minimal amount of 0.5 g L^{-1} YE was still added.

3.5.7.1 Failed Reactor Startup due to Untimely Initiation of Feed

Remarkably, the parallel start-ups of R8-F1 and R11-R1 exhibited contrasting outcomes (Attachment Fig. 20 and 23). R8-F1 experienced a delayed growth in the first 16 hours, while R11-R1 exhibited a faster growth with an OD of 0.137 and a calculated growth rate (μ) of 0.036 h^{-1} during the same period. Within the subsequent 5 hours, R8-F1's growth began, reaching an OD of 0.100 and a calculated μ of 0.057 h^{-1}, whereas R11-F1 ceased to grow, with the online CO_2 signal decreasing, indicating the end of the batch phase. As a result, the feed was initiated for R11-F1 with a dilution rate of 0.025 h^{-1}. Meanwhile, R8-F1 continued in the batch phase until 46 hours, where an OD of 0.219 and a calculated μ of 0.03 h^{-1} were measured. At this point, the dilution rate was adjusted to 0.025 h^{-1} as well.

Unfortunately, the cell density in R11-F1 decreased by 40 % to an OD of 0.083. Nevertheless, the CO_2 off-gas indicated ongoing cellular activity, leading to the decision to maintain a constant dilution rate. However, over the following two weeks, the OD, CO_2, formate, and acetate measurements fluctuated without reaching a stable value expected in chemostat mode.

Conversely, R8-F1 reached its peak OD of 0.377 after 71 hours, approximately 24 hours after starting the feed. Subsequently, the OD gradually declined, stabilizing at around 0.230. Throughout this period, CO_2, formate, and acetate measurements remained constant, enabling the establishment of a balance period lasting approximately 7 days, during which steady-state calculations were performed.

Despite the successes observed in the bioreactor experiments, R11-F1, unfortunately, failed to achieve steady-state conditions, highlighting the need for further improvements in the experimental setup. To address this challenge and enhance the reliability of future experiments, several key suggestions are proposed:

- Sampling during the batch phase at shorter time intervals.

- Analyze substrate concentration determination in the HPLC before initiating the feed. This provides certainty about the amount of substrate already consumed.
- If OD values continuously decrease after starting the feed, the feed supply should be halted to prevent cell washout.
- With a backup pre-culture, the reactor volume can be exchanged and promptly re-inoculated, avoiding the need for dismantling, autoclaving, cleaning, and re-equipping the reactor.

3.5.7.2 Cell Death Resulting from Inadvertent Feed Interruption.

Following the successful operation of R8-F1, a decision was made to elevate the feed concentration from 200 to 500 mM formate, a step aimed at exploring the system's response under altered conditions. As outlined in the material and methods section, the revised Feed solution was prepared. During the fermentation process, a short interruption was intended by changing the feed bottle and subsequently connecting it to the reactor. Upon restarting the pump, the feed was expected to flow into the reactor in a gradual and controlled manner, as observed in previous runs.

However, a setback emerged during the experiment. Hours later, upon inspecting the real-time monitoring and control system (Lucullus), an unexpected interruption in the feed supply was detected. Subsequent investigation revealed that the feed flow had been stopped. The situation was promptly addressed, and the feed pump was fixed the following day. Against all expectations, an unforeseen consequence emerged as the optical density of the culture precipitously declined from 0.268 to 0.089. This decline persisted in the ensuing days, concomitant with an accumulation of formate within the reactor. Notably, even turning off the feed failed to stimulate growth, thereby leading to the decision to halt the operation of the reactor.

The occurrence of cell death after 14 hours without feed was an unexpected observation. The dramatic impact of this relatively short interruption in nutrient supply highlighted the remarkable sensitivity of the microbial culture in the environmental conditions. This unforeseen outcome underscores the critical role that continuous nutrient availability plays in sustaining the viability and growth of the microorganisms within the bioreactor. Furthermore, this observation emphasizes the significance of precise operational planning and execution in bioprocessing. Continuous monitoring of essential parameters, such as nutrient availability, in order to promptly detect any deviations from the desired conditions is of great importance.

In summary, the discovery that a relatively short interruption in feed supply led to cell death serves as a valuable lesson in understanding the relationship between nutrient

availability and microbial viability. This experience highlights the importance of exercising with patience when implementing changes within the bioprocessing system.

3.5.7.3 No growth in the batch phase due to too high stirrer speed

The initiation of continuous bioreactor operations represents a critical phase for the cultivation of *A. woodii* under the constraints of limited conditions. The startup phase of two parallel inoculated reactors with an initial optical density of 0.09 unexpectedly exhibited a decrease in biomass over a span of 6 days. A speculation emerged, attributing this growth stagnation to the potential effects of shear stress induced by agitation. This hypothesis relies on observations from serum bottles, wherein cells clump together during growth. This led to the notion that cellular aggregation might have an impact of growth in the reactor environment. Consequently, this speculation was addressed by reducing the stirrer speed.

Both R8-F2 and R11-F2 (Figure 31 and 32), initiated with the standard stirring speed of 150 rpm, exhibited a decline in OD_{600} within the initial 24 hours. In response to this trend, adjustments were made to the stirring speed. The stirrer speed for R11-F2 was reduced to 50 rpm after 26 hours, and the same adjustment was implemented for R8-F2 after 42 hours. This alteration in agitation yielded remarkable outcomes. Following these adjustments, a rapid and substantial increase in biomass was observed, with one reactor displaying a growth rate of 0.087 h^{-1} and the other exhibiting an even more remarkable μ of 0.313 h^{-1} during the batch phase. After this notable increase in biomass, the decision was taken to initiate feed flow. At a later stage, the stirrer speed was restored to 150 rpm. Both reactors achieved a steady state within a span of 150 hours after the feed initiation.

This experience has induced valuable lessons and insights. Notably, it was identified that a reduction in agitation during the initial batch phase can effectively stimulate biomass growth. However, it is essential to exercise caution, as insufficient agitation could potentially trigger the formation of a biofilm on reactor walls, stirrer blades, and baffles. This underscores the importance of observation and monitoring during such phases. Furthermore, despite the rapid biomass increase, there was barely any increase in acetate production.

In light of these findings, several suggestions can be proposed. Consideration should be given to implementing a lower stirrer speed during the batch phase to facilitate enhanced biomass growth, but with a watchful eye on the potential biofilm formations. Additionally, an optimal timing for the initiation of feed start is crucial.

3.5.7.4 Failed Feed Concentration Switch from 200 to 500 mM formate

The attempt to switch the feed concentration from 200 to 500 mM formate resulted in the failure of both reactors to effectively metabolize this higher formate concentration.

Instead, both reactors exhibited a problematic accumulation of formate, reaching levels of 300 mM and 450 mM, respectively. To address this issue, the decision was made to halt the feed flow, acknowledging that the reactors were unable to cope with the elevated formate load.

To spur biomass growth and address the formate accumulation, 1 g L^{-1} fructose was introduced, coupled with a successful adjustment of the stirrer speed to 50 rpm for one reactor. This adjustment facilitated the consumption of accumulated formate. Following this corrective measure, the feed was resumed with a reduced concentration of 300 mM and a dilution rate of 0.025 h^{-1}. Remarkably, this reactor achieved a steady state four days after the feed resumption.

There are some lessons learnt from these observations. Firstly, it is apparent that abrupt changes in feed concentration can pose significant challenges to microbial metabolism. This underscores the necessity for gradual transitions when altering nutrient inputs. Furthermore, the efficacy of using alternative carbon sources, such as fructose, to punctually induce biomass growth was shown.

3.5.7.5 Formation of a Biofilm

The formation of a persistent biofilm within the reactor led to challenges in accurately quantifying the biomass present in the system. This biofilm emerged when the dilution rate reached 0.1 h^{-1} and remained in place after attempts to mitigate its presence through an increase in stirrer speed. As the process continued, the biofilm progressively expanded, eventually obstructing the view inside the reactor.

This biofilm's presence presented both positive and negative implications. On a positive note, the biofilm acted as a cell retention mechanism. A subset of cells permanently remained within the reactor as biofilm matrix, resulting in elevated acetate productivity. Conversely, the biofilm posed challenges in data interpretation, particularly with respect to biomass-specific rates, making these metrics unreliable. Consequently, the focus shifted to using volumetric rates as a more representative measure. Additionally, the role of the biofilm in enabling *A. woodii* to endure high dilution rates, such as 0.2 h^{-1}, is unclear. Time and project constraints precluded any additional increase of the dilution rate. Nonetheless, it appeared plausible that the dilution rate could have been further elevated. The observed capacity for elevated rates showcased *A. woodii's* adaptability. This biofilm-induced situation underscores the necessity for deeper insights into the underlying mechanisms driving cell aggregation and adhesion to reactor surfaces. A more comprehensive understanding of these phenomena is crucial for process design and optimization.

For comparative purposes, prior investigations have reported maximum growth rates of 0.08, 0.05, and 0.13 h^{-1} during batch cultivation of *A. woodii* (Demler & Weuster-Botz,

2011; Novak et al., 2021; Straub et al., 2014). These rates were achieved when employing a combination of hydrogen and carbon dioxide, and in the latter case, the addition of carbon monoxide, within a medium containing yeast extract. Another study explored batch cultivation using a complex medium supplemented with 200 mM formate, resulting in the observation of a maximum growth rate of 0.12 h^{-1} (Moon et al., 2021).

In summary, while the biofilm presented challenges in terms of data interpretation, it also significantly enhanced the productivity of *A. woodii* and likely played a crucial role in preventing cell washout at higher dilution rates.

A study by Steger et. al., 2017 delivers an innovative approach to enhance microbial productivity and prevent cell washout in a continuous gas fermentation. This method involved the implementation of a linen cylinder, strategically placed to accumulate and immobilize bacterial cells and therefore facilitate cell retention. This technique promotes the retention of *A. woodii* within the bioreactor, ensuring sustained microbial growth and enabling efficient bioprocessing. The results of this study showcased the efficacy of a simple and cheap linen net-based cell retention strategy (Steger et al., 2017).

Conclusion

Throughout the course of this thesis, our investigation into the viability of cultivating *A. woodii* in a bioreactor with formate as the exclusive carbon and energy source, within a chemically defined medium, has yielded a wealth of valuable insights into the metabolic opportunities and challenges inherent to this subject. We started with preliminary tests in 125 mL serum bottles, which provided an initial comprehension into the feasibility under the desired conditions. As we continued our investigation, we explored different metabolic situations, such as substrate variations and vitamin availability, facing both the flexibility and challenges that come with this biochemical system. Our path then expanded to encompass continuous bioreactor experiments, where formate concentrations and dilution rates were systematically elevated. This has painted an extensive picture of *A. woodii's* metabolic adaptability and the scope of acetate bioproduction.

The genealogical tree shows the evolutionary strain enhancement over multiple passages and time. The starting point of this genealogy is a non adapted strain of *Acetobacterium woodii*. Figure 5 and 6 presents a graphically description of the adaptive laboratory evolution. A wide range of conditions is included in this progression, involving variations in media, carbon source compositions such as formate and CO, and strategies for vitamin supplementation. The genealogy portrays instances where final optical densities exhibit an increasing trend over several passages until they ultimately stabilize at a plateau. However, the lineage exclusively relying on formate as the sole carbon and energy source demonstrated a lack of substantial fnal biomass increase across conducted passages. These carefully developed lineage of subcultures provided the solid foundation for the subsequent deployment in continuous bioreactor cultivations.

The investigation commenced by contrasting two chemically defined media: one featuring a carbonate buffer and the other a phosphate buffer. The favored usage of a phosphate-buffered medium stemmed from the disadvantageous effects of carbonate within the system. The elevated sodium carbonate concentration posed challenges in terms of sodium ion concentration, with potential implications for the chemiosmotic ATP synthesis mechanism. Additionally, the introduction of CO_3^- as an extra carbon source introduced complexities in metabolic pathways, leading to potentially undesired cellular uptake. The utilization of a phosphate-buffered medium effectively circumvented these challenges. Even though, experimental outcomes revealed a higher final optical density (OD_{600}) in the carbonate medium, the decision to exclude carbonate buffer usage and instead employ a phosphate-buffered medium for all subsequent experiments and assays emerged. This choice ensures consistency in the buffer system, aligning the conditions in the serum bottles with those in the bioreactor cultivation.

The synergistic utilization of formate and CO was carried out in serum bottle experiments. Three distinct modifications were examined, involving 100 mM formate in combination with either 25 % or 50 % CO, alongside a condition reliant solely on 25 % CO as substrates. The growth profiles across three passages, as depicted in Figure 8, revealed an inhibition phenomenon when combining formate and CO: a slightly higher final optical density manifested when the gas phase contained 25 % CO compared to 50 % CO, despite the presence of less carbon for growth. This paradox is attributed to the inhibitory impact of CO on specific enzymes integral to the WLP (Schuchmann & Müller, 2014a). Considering the lack of growth benefits with CO content exceeding 25 %, this concentration was selected for subsequent strain selection. In the presence of 100 mM formate and 25 % CO, the final optical density (OD_{600}) is measured at 0.64 ± 0.09, with a corresponding growth rate calculated to be 0.053 ± 0.01 h^{-1}.

However, the sole use of carbon monoxide as the carbon and energy source yielded no observable growth. This outcome stems from the inhibitory effects of CO on two hydrogenase enzymes. One of these enzymes, an electron-bifurcating hydrogenase, participates in ferredoxin and NAD^+ reduction. The second hydrogenase forms a crucial component of the HDCR complex, responsible for converting CO_2 to formate using H_2 or ferredoxin as electron donors. The presence of CO was found to hinder formate production via the HDCR complex from CO_2, thus impeding the initial step of the methyl branch of the Wood-Ljungdahl pathway(Bertsch & Müller, 2015; Schuchmann & Müller, 2013).

Further experiments explored formate as the exclusive carbon source in serum bottles. Under 100 mM formate conditions, a mean OD_{600} of 0.143 ± 0.029 was observed. The calculated growth rate is 0.03 h^{-1}, exhibiting a standard deviation of 7.5 %. Although seemingly low, this value can be rationalized by the absence of yeast extract, gaseous carbon, and energy sources in the medium. These specific conditions in a phosphate buffered medium without yeast extract and formate as the sole carbon and energy source have remained unexplored. Subsequently, formate concentrations were elevated to 200 mM in serum bottle experiments. Upon comparing the resulting final biomass concentration and growth rate under 100 mM and 200 mM formate conditions, a concentration of 100 mM was pursued due to a slightly lower optical density and growth rate at 200 mM formate levels.

Vitamins play various roles in biochemistry, and many are necessary for biochemical and metabolic functions. Different vitamins act as precursors for enzymes, and organisms uniquely depend on their specific vitamin compositions. A study by Balch et. al., hinted that *A. woodii* might need only one vitamin, namely pantothenate (Balch et al., 1977). To corroborate this discovery, carried out nearly half a century ago, experimental validation was conducted employing both Ca-pantothenate alone and complete vitamin

supplementation. The mean values of the final optical density after several passages are found to be 0.64 and 0.61, respectively. These numbers come with relative standard deviations of 14 % and 15 %. The mean growth rates for Ca-pantothenate and full vitamin supply showed a value 0.053 and 0.058, respectively – each accompanied by a relative standard deviation of 19 %. These values reveal no discernible difference between both conditions. This empirical evidence firmly establishes *A. woodii's* exclusive need for pantothenate as its sole vitamin requirement. Conceivably, the coenzymes essential for cellular processes can be synthesized via alternative metabolic pathways in the absence of their corresponding vitamin precursors. This revelation holds potential for industrial applications, offering insights into cost-effective strategies by the use of a minimal vitamin amount.

Continuous bioproduction offers an uninterrupted and fluid manufacturing process that enhances productivity by eliminating gaps between batches and facilitating a consistent input of raw materials. This operational mode ensures unwavering product quality through real-time monitoring and adjustments. In the exploration of continuous acetate bioproduction with *A. woodii*, the dynamics of continuous clultures play a pivotal role in comprehending microbial behavior and optimizing desired outcomes. This investigation delves into the influence of varying formate concentrations and dilution rates and its metabolic response. Starting at a dilution rate of 0.025 h^{-1} and a formate concentration of 200 mM, the study concludes at a dilution rate of 0.2 h^{-1} and a formate concentration of 300 mM. The biomass concentration demonstrates considerable variability under the observed dilution rates and a concentration of 200 mM formate. This variability may stem from cells' adaptability to a wide substrate range when the dilution rate remains below their maximum growth rate within the given conditions. Despite the biomass concentration's variability, experiments conducted under 200 mM formate concentration exhibit remarkable consistency among results. Under 300 mM formate feed a formation of biofilm occurs at 0.1 h^{-1} and intensifies with increasing dilution rates, making exact biomass concentration measurement unreachable. Nonetheless, volumetric rates demonstrate a linear correlation with dilution rates, giving rise to empirical correlations between dilution rate and volumetric rates, evident for constant formate feed concentrations of 200 and 300 mM. An optimum acetate yield at dilution rates between 0.1 and 0.15 h^{-1} is observed at 300 mM formate concentration, with a measured value of 0.223 ± 0.002 mol mol^{-1}. The system's robustness, as evidenced by its ability to maintain stability and functionality even at high dilution rates of up to 0.2 h^{-1}, is likely attributed to the development of a biofilm within the bioreactor. The highest acetate rate is observed at a dilution rate of 0.2 h^{-1}, resulting in 12.64 mmol L^{-1} h^{-1} and a concentration of 3.77 g L^{-1}. The highest acetate concentration was recorded at 0.1 h^{-1} dilution rate, featuring 4.1 g L^{-1} and a volumetric rate of 6.94 mmol L^{-1} h^{-1}.

Although currently speculative, there is a plausible possibility of extending the upper limit of both dilution rate and formate concentration based on the existing experimental context.. However, the feasibility of such an extension without the emergence of a biofilm remains an unanswered question. Nevertheless, the biofilm adds an unexpected positive dimension. By firmly adhering to the reactor's walls, the biofilm actively operates as a retention system, facilitating the realization of elevated dilution rates and higher acetate production rates, thereby enhancing the potential of the entire bioproduction process.

Alongside continuous bioprocessing with *A. woodii* introduces an array of unwanted interactions and dynamic hurdles. To enhance microbial growth and optimize productivity within constrained conditions has yielded in several insightful recommendations. Firstly, frequent sampling during the batch phase at shorter intervals enhances process insight, capturing rapid shifts in microbial behavior for more precise control. Before initiating feed, conduct substrate concentration analysis using HPLC to ensure accurate knowledge of remaining substrate, guiding informed decisions on feed initiation and preventing imbalances. Mitigate downtime by maintaining a backup pre-culture, allowing for rapid reactor exchange and re-inoculation in case of issues. A notable discovery is the induction of biomass growth through the implementation of lower stirrer speeds during the batch phase. Due to low agitation the diminished shear stress at reactor surfaces intensifies the formation of a biofilm, which must be controlled and prevented. Gradually transition feed concentrations to prevent disruptions in microbial metabolism, ensuring smoother adaptation and sustained productivity. Utilize alternative carbon sources, such as fructose, for punctual biomass growth induction. Lastly, recognize the dual role of biofilm formation, which, while posing data interpretation challenges, enhances *A. woodii's* productivity as a cell retention facility in the process dynamics.

In conclusion, acetogens, exemplified by *A. woodii*, have the potential to serve as a robust and sustainable biological conversion platform for CO_2 and its derived C1 molecules, notably formate. Their reductive metabolism opens new ways for implementing CO_2 reduction strategies at an industrial scale. Acetogens provides a promising framework for sustainable production processes, offering a solution to mitigate greenhouse gas emissions. The transformative potential of acetogens positioning them as key players in the quest for environmentally and economically viable technologies.

Bibliography

Adamu, A., Isaacs, M., Boodhoo, K., & Abegão, F. R. (2023). Investigation of Cu/TiO2 synthesis methods and conditions for CO2 photocatalytic reduction via conversion of bicarbonate/carbonate to formate. *Journal of CO2 Utilization*, *70*, 102428. https://doi.org/10.1016/j.jcou.2023.102428

Balch, W. E., Schoberth, S., Tanner, R. S., & Wolfe, R. S. (1977). Acetobacterium, a New Genus of Hydrogen-Oxidizing, Carbon Dioxide-Reducing, Anaerobic Bacteria. In *International Association of Microbiological Societies* (Vol. 27, Issue 4).

Basen, M., & Müller, V. (2017). "Hot" acetogenesis. In *Extremophiles* (Vol. 21, Issue 1, pp. 15–26). Springer Tokyo. https://doi.org/10.1007/s00792-016-0873-3

Bender, D. A. (2003). *Nutritional Biochemistry of the Vitamins* (2nd ed.). Cambridge University Press. https://doi.org/10.1017/CBO9780511615191

Bertsch, J., & Müller, V. (2015). CO metabolism in the acetogen Acetobacterium woodii. *Applied and Environmental Microbiology*, *81*(17), 5949–5956. https://doi.org/10.1128/AEM.01772-15

Biegel, E., & Müller, V. (2010). Bacterial Na$^+$-translocating ferredoxin:NAD$^+$ oxidoreductase. *Proceedings of the National Academy of Sciences*, *107*(42), 18138–18142. https://doi.org/10.1073/pnas.1010318107

Bulushev, D. A., & Ross, J. R. H. (2018). Towards Sustainable Production of Formic Acid. In *ChemSusChem* (Vol. 11, Issue 5, pp. 821–836). Wiley-VCH Verlag. https://doi.org/10.1002/cssc.201702075

Cannon, A. T., & Saouma, C. T. (2021). Ru catalyzed hydrogenation of CO2 to formate under basic and acidic conditions. *Polyhedron*, *207*. https://doi.org/10.1016/j.poly.2021.115375

Cheng, H. H., Syu, J. C., Tien, S. Y., & Whang, L. M. (2018). Biological acetate production from carbon dioxide by Acetobacterium woodii and Clostridium ljungdahlii: The effect of cell immobilization. *Bioresource Technology*, *262*, 229–234. https://doi.org/10.1016/j.biortech.2018.04.069

Cotton, C. A., Claassens, N. J., Benito-Vaquerizo, S., & Bar-Even, A. (2020). Renewable methanol and formate as microbial feedstocks. *Current Opinion in Biotechnology*, *62*, 168–180. https://doi.org/10.1016/j.copbio.2019.10.002

Demler, M., & Weuster-Botz, D. (2011). Reaction engineering analysis of hydrogenotrophic production of acetic acid by Acetobacterium woodii. In *Biotechnology and Bioengineering* (Vol. 108, Issue 2, pp. 470–474). https://doi.org/10.1002/bit.22935

Dönig, J., & Müller, V. (2018). *Alanine, a Novel Growth Substrate for the Acetogenic Bacterium Acetobacterium woodii*. https://doi.org/10

Drake, H. L., Gößner, A. S., & Daniel, S. L. (2008). Old acetogens, new light. *Annals of the New York Academy of Sciences*, *1125*, 100–128. https://doi.org/10.1196/annals.1419.016

European Chemical Agency. (2023, August 25). *Biodegradation of Formic Acid*. Https://Echa.Europa.Eu/Registration-Dossier/-/Registered-Dossier/15127/5/3/3.

Godley, A. R., Linnett, P. E., & Robinson, J. P. (1990). The effect of carbon dioxide on the growth kinetics of fructose-limited chemostat cultures of A cetobacterium woodii D S M 1030. In *Archives of Microbiology* (Vol. 154). Springer-Verlag.

Hess, V., Schuchmann, K., & Müller, V. (2013). The ferredoxin: NAD+ Oxidoreductase (Rnf) from the acetogen acetobacterium woodii requires na+ and is reversibly coupled to the membrane potential. *Journal of Biological Chemistry*, *288*(44), 31496–31502. https://doi.org/10.1074/jbc.M113.510255

Imkamp, F., & Müller, V. (2002). Chemiosmotic energy conservation with Na+ as the coupling ion during hydrogen-dependent caffeate reduction by Acetobacterium woodii. *Journal of Bacteriology*, *184*(7), 1947–1951. https://doi.org/10.1128/JB.184.7.1947-1951.2002

Jacob Bryde, T. S. (2014, April). *Acetobacterium woodii*. Jacob Bryde and Tim Stieve.

Karekar, S., Stefanini, R., & Ahring, B. (2022). Homo-Acetogens: Their Metabolism and Competitive Relationship with Hydrogenotrophic Methanogens. In *Microorganisms* (Vol. 10, Issue 2). MDPI. https://doi.org/10.3390/microorganisms10020397

Khan, I., Hou, F., & Le, H. P. (2021). The impact of natural resources, energy consumption, and population growth on environmental quality: Fresh evidence from the United States of America. *Science of the Total Environment*, *754*. https://doi.org/10.1016/j.scitotenv.2020.142222

Lemaire, O. N., Jespersen, M., & Wagner, T. (2020). CO2-Fixation Strategies in Energy Extremophiles: What Can We Learn From Acetogens? In *Frontiers in Microbiology* (Vol. 11). Frontiers Media S.A. https://doi.org/10.3389/fmicb.2020.00486

Litty, D., Kremp, F., & Müller, V. (2022). One substrate, many fates: different ways of methanol utilization in the acetogen <scp> *Acetobacterium woodii* </scp>. *Environmental Microbiology*, *24*(7), 3124–3133. https://doi.org/10.1111/1462-2920.16011

Martin, W. F. (2020). Older Than Genes: The Acetyl CoA Pathway and Origins. In *Frontiers in Microbiology* (Vol. 11). Frontiers Media S.A. https://doi.org/10.3389/fmicb.2020.00817

Merino-Garcia, I., Tinat, L., Albo, J., Alvarez-Guerra, M., Irabien, A., Durupthy, O., Vivier, V., & Sánchez-Sánchez, C. M. (2021). Continuous electroconversion of CO2 into formate using 2 nm tin oxide nanoparticles. *Applied Catalysis B: Environmental*, *297*. https://doi.org/10.1016/j.apcatb.2021.120447

Moon, J., Dönig, J., Kramer, S., Poehlein, A., Daniel, R., & Müller, V. (2021). Formate metabolism in the acetogenic bacterium Acetobacterium woodii. *Environmental Microbiology*, *23*(8), 4214–4227. https://doi.org/10.1111/1462-2920.15598

Müller, V. (2003). Energy Conservation in Acetogenic Bacteria. In *Applied and Environmental Microbiology* (Vol. 69, Issue 11, pp. 6345–6353). https://doi.org/10.1128/AEM.69.11.6345-6353.2003

Neuendorf, C. S., Vignolle, G. A., Derntl, C., Tomin, T., Novak, K., Mach, R. L., Birner-Grünberger, R., & Pflügl, S. (2021). A quantitative metabolic analysis reveals Acetobacterium woodii as a flexible and robust host for formate-based bioproduction. *Metabolic Engineering*, *68*, 68–85. https://doi.org/10.1016/j.ymben.2021.09.004

Novak, K., Neuendorf, C. S., Kofler, I., Kieberger, N., Klamt, S., & Pflügl, S. (2021). Blending industrial blast furnace gas with H2 enables Acetobacterium woodii to efficiently co-utilize CO, CO2 and H2. *Bioresource Technology*, *323*. https://doi.org/10.1016/j.biortech.2020.124573

Patwa, N., Sivarajah, U., Seetharaman, A., Sarkar, S., Maiti, K., & Hingorani, K. (2021). Towards a circular economy: An emerging economies context. *Journal of Business Research*, *122*, 725–735. https://doi.org/10.1016/j.jbusres.2020.05.015

Poehlein, A., Schmidt, S., Kaster, A. K., Goenrich, M., Vollmers, J., Thürmer, A., Bertsch, J., Schuchmann, K., Voigt, B., Hecker, M., Daniel, R., Thauer, R. K., Gottschalk, G., & Müller, V. (2012). An ancient pathway combining carbon dioxide fixation with the generation and utilization of a sodium ion gradient for ATP synthesis. *PLoS ONE*, *7*(3). https://doi.org/10.1371/journal.pone.0033439

Ragsdale, S. W., & Pierce, E. (2008). Acetogenesis and the Wood-Ljungdahl pathway of CO2 fixation. In *Biochimica et Biophysica Acta - Proteins and Proteomics* (Vol. 1784, Issue 12, pp. 1873–1898). https://doi.org/10.1016/j.bbapap.2008.08.012

Sánchez-Andrea, I., Guedes, I. A., Hornung, B., Boeren, S., Lawson, C. E., Sousa, D. Z., Bar-Even, A., Claassens, N. J., & Stams, A. J. M. (2020). The reductive glycine pathway allows autotrophic growth of Desulfovibrio desulfuricans. *Nature Communications*, *11*(1). https://doi.org/10.1038/s41467-020-18906-7

Schuchmann, K., & Müller, V. (2012). A bacterial electron-bifurcating hydrogenase. *Journal of Biological Chemistry*, *287*(37), 31165–31171. https://doi.org/10.1074/jbc.M112.395038

Schuchmann, K., & Müller, V. (2013). Direct and Reversible Hydrogenation of CO2 to Formate by a Bacterial Carbon Dioxide Reductase. *Science*, *342*(6164), 1382–1385. https://doi.org/10.1126/science.1244758

Schuchmann, K., & Müller, V. (2014a). A new enzyme for the direct hydrogenation of CO2: Alternative energies. *BioSpektrum*, *20*(2), 240–241. https://doi.org/10.1007/s12268-014-0434-1

Schuchmann, K., & Müller, V. (2014b). Autotrophy at the thermodynamic limit of life: A model for energy conservation in acetogenic bacteria. In *Nature Reviews Microbiology* (Vol. 12, Issue 12, pp. 809–821). Nature Publishing Group. https://doi.org/10.1038/nrmicro3365

Schuchmann, K., Vonck, J., & Müller, V. (2016). A bacterial hydrogen-dependent CO2 reductase forms filamentous structures. *FEBS Journal*, *283*(7), 1311–1322. https://doi.org/10.1111/febs.13670

Steger, F., Rachbauer, L., Windhagauer, M., Montgomery, L. F. R., & Bochmann, G. (2017). Optimisation of continuous gas fermentation by immobilisation of acetate-producing Acetobacterium woodii. *Anaerobe*, *46*, 96–103. https://doi.org/10.1016/j.anaerobe.2017.06.010

Straub, M., Demler, M., Weuster-Botz, D., & Dürre, P. (2014). Selective enhancement of autotrophic acetate production with genetically modified Acetobacterium woodii. *Journal of Biotechnology*, *178*(1), 67–72. https://doi.org/10.1016/j.jbiotec.2014.03.005

Tashiro, T., Ishida, A., Hori, M., Igisu, M., Koike, M., Méjean, P., Takahata, N., Sano, Y., & Komiya, T. (2017). Early trace of life from 3.95 Ga sedimentary rocks in Labrador, Canada. *Nature*, *549*(7673), 516–518. https://doi.org/10.1038/nature24019

Ueno, Y., Yamada, K., Yoshida, N., Maruyama, S., & Isozaki, Y. (2006). Evidence from fluid inclusions for microbial methanogenesis in the early Archaean era. *Nature*, *440*(7083), 516–519. https://doi.org/10.1038/nature04584

Vanholme, B., Desmet, T., Ronsse, F., Rabaey, K., Van Breusegem, F., De Mey, M., Soetaert, W., & Boerjan, W. (2013). Towards a carbon-negative sustainable bio-based economy. In *Frontiers in Plant Science* (Vol. 4, Issue JUN). Frontiers Research Foundation. https://doi.org/10.3389/fpls.2013.00174

Velenturf, A. P. M., & Purnell, P. (2021). Principles for a sustainable circular economy. In *Sustainable Production and Consumption* (Vol. 27, pp. 1437–1457). Elsevier B.V. https://doi.org/10.1016/j.spc.2021.02.018

Wood, H. G., Ragsdale, S. W., & Pezacka, E. (1986). The acetyl-CoA pathway of autotrophic growth. *FEMS Microbiology Letters*, *39*(4), 345–362. https://doi.org/10.1111/j.1574-6968.1986.tb01865.x

Yishai, O., Lindner, S. N., Gonzalez de la Cruz, J., Tenenboim, H., & Bar-Even, A. (2016). The formate bio-economy. *Current Opinion in Chemical Biology*, *35*, 1–9. https://doi.org/10.1016/j.cbpa.2016.07.005

Zhou, L., Yao, C., Ma, W., Hu, J., Wu, Y., Zhang, Z., & Hu, X. (2021). CO_2 hydrogenation to formate catalyzed by highly stable and recyclable carbene-iridium under mild condition. *Journal of CO2 Utilization*, *54*. https://doi.org/10.1016/j.jcou.2021.101769

Attachment
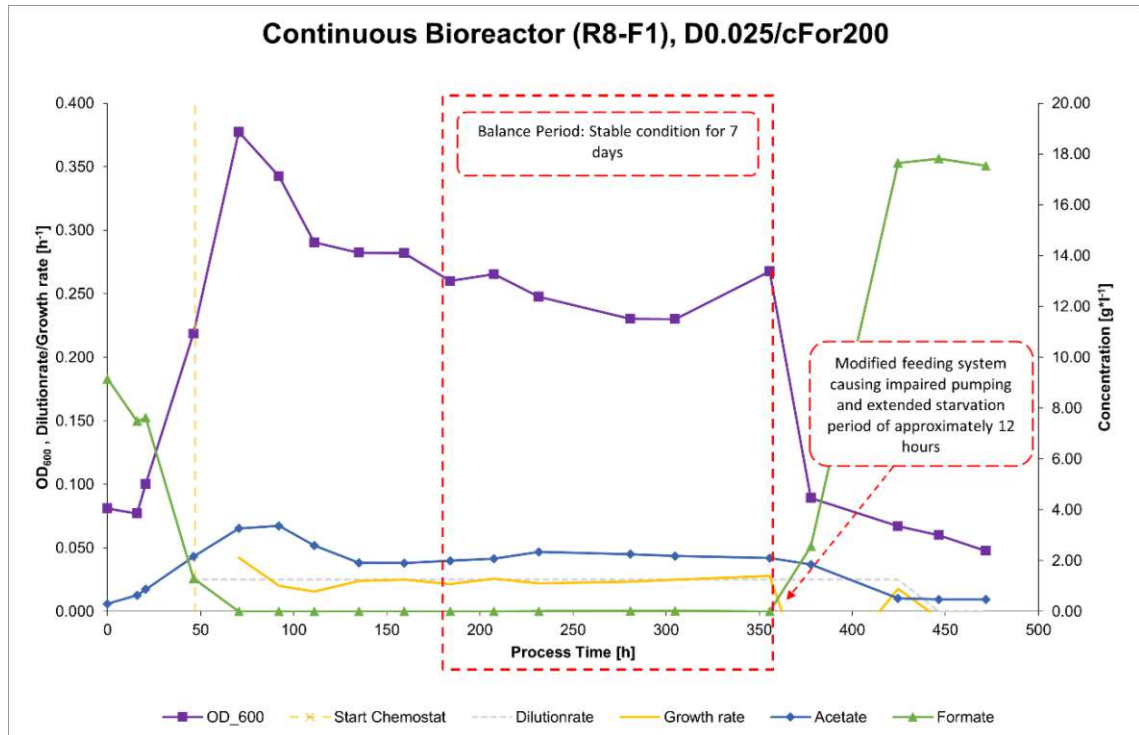
Figure 20: Continuous Bioreactor (R8-F1), D = 0.025 h^{-1}; c$_{For}$ = 200 mM
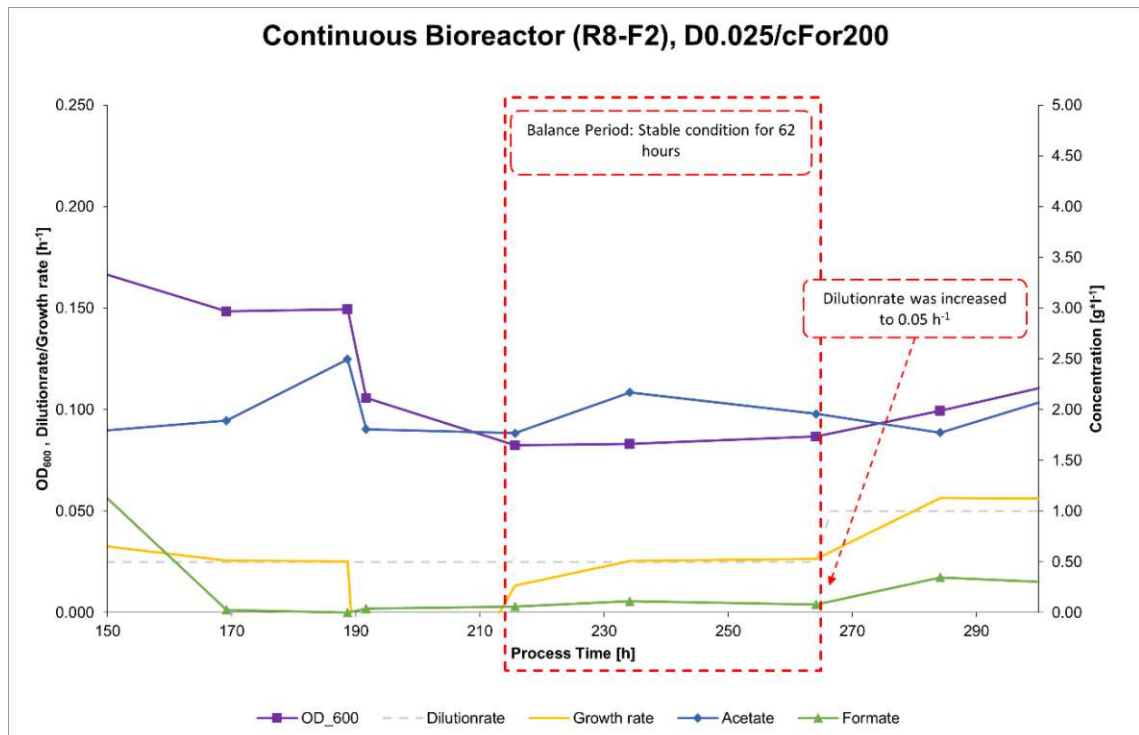
Figure 21: Continuous Bioreactor (R8-F2), D = 0.025 h^{-1}; c$_{For}$ = 200 mM
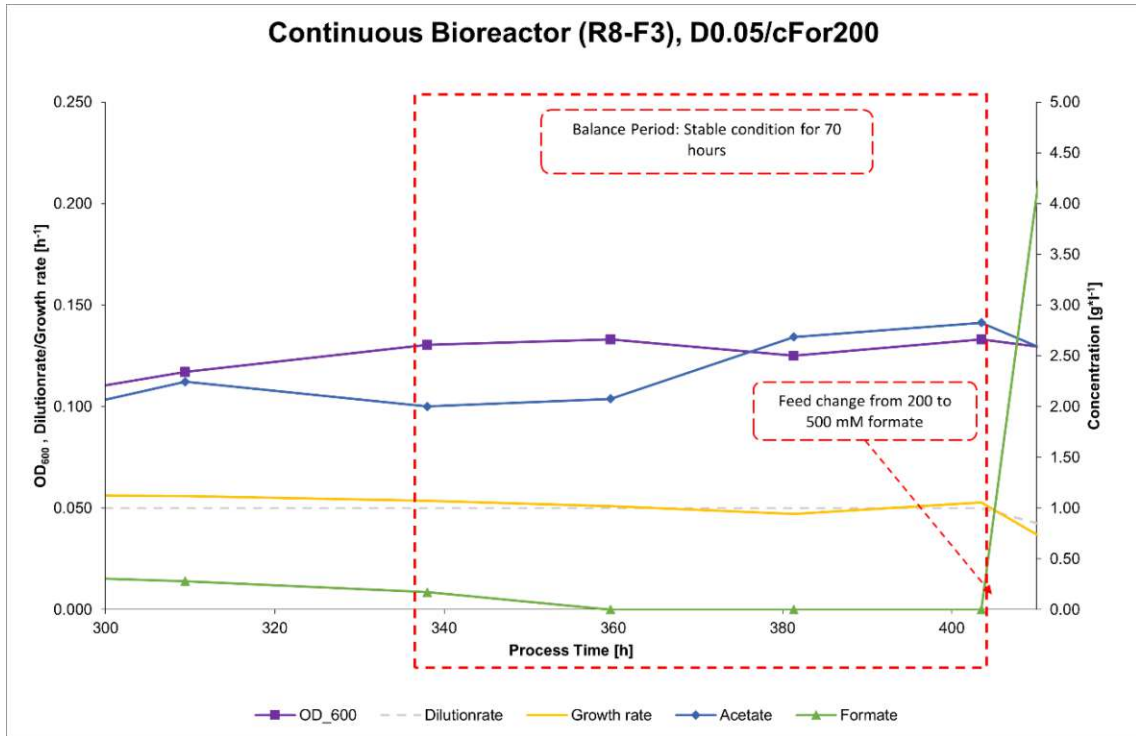
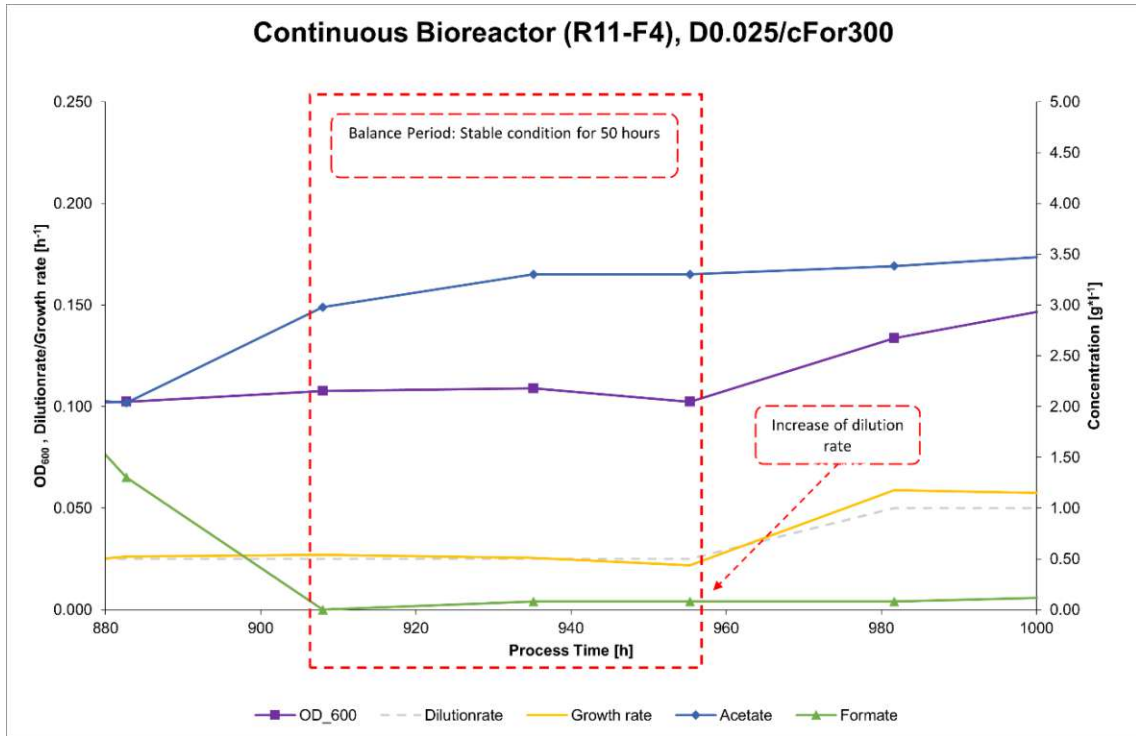Figure 22: Continuous Bioreactor (R8-F3), D = 0.050 h^{-1}; c$_{For}$ = 200 mM
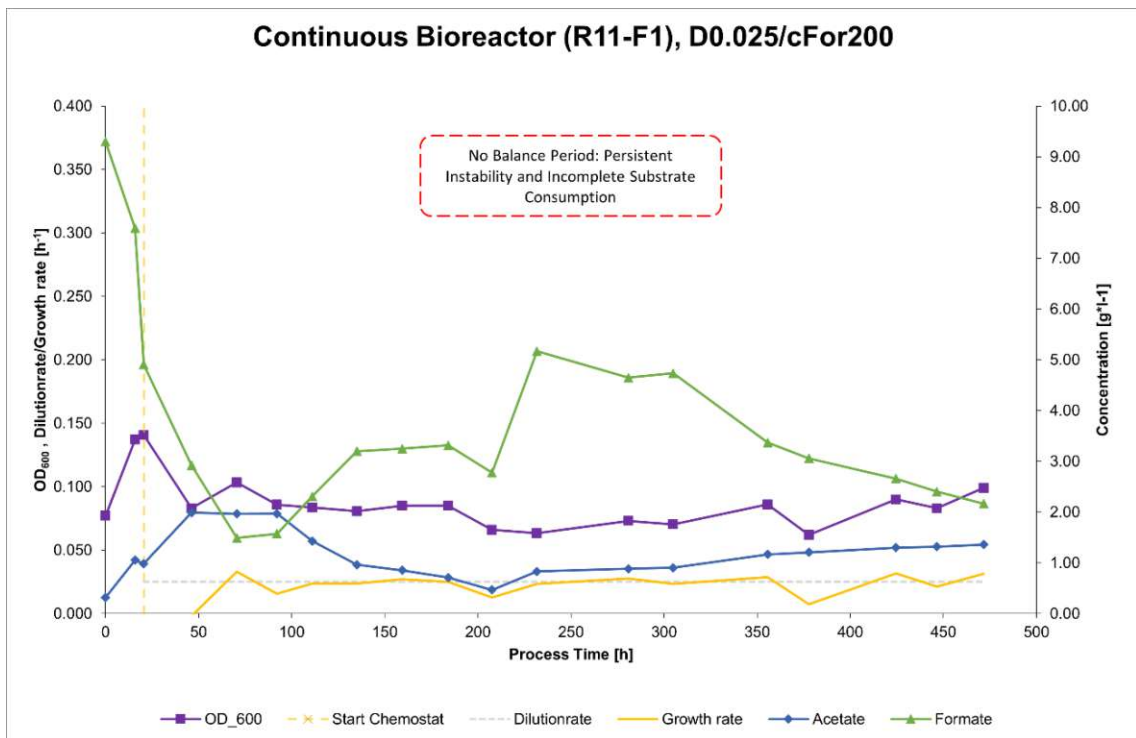
Figure 23: Continuous Bioreactor (R11-F1), D = 0.025 h^{-1}; c$_{For}$ = 200 mM
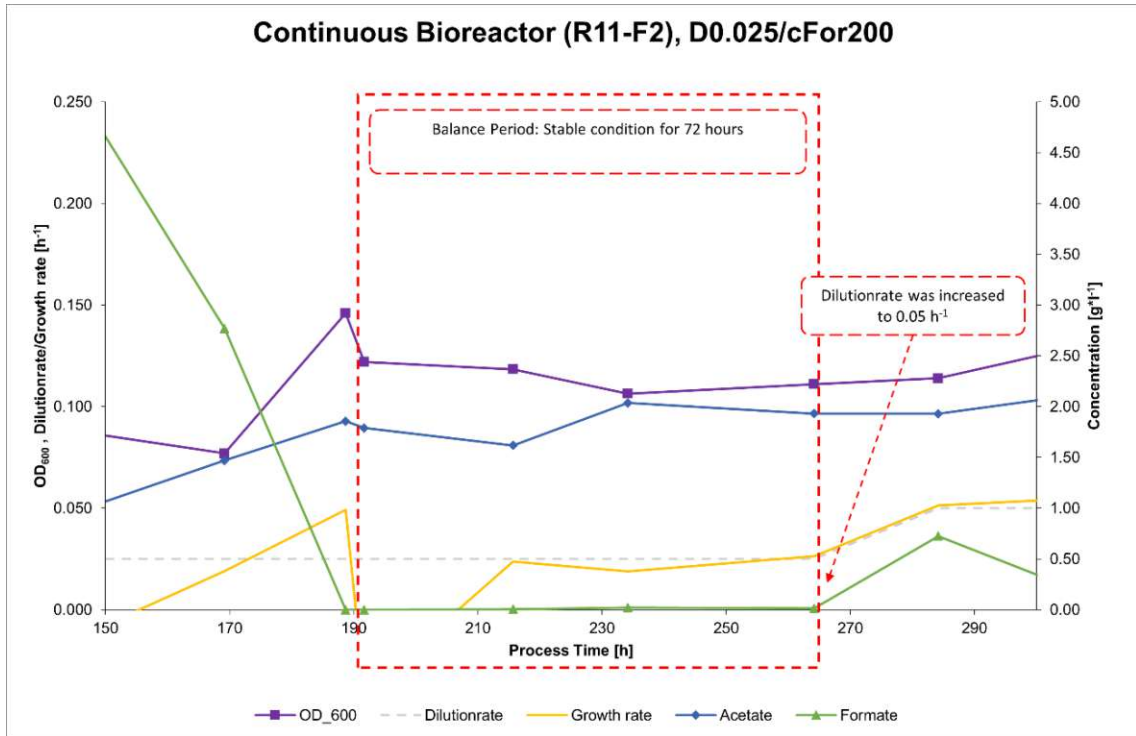
Figure 24: Continuous Bioreactor (R11-F2), D = 0.025 h^{-1}; c$_{For}$ = 200 mM
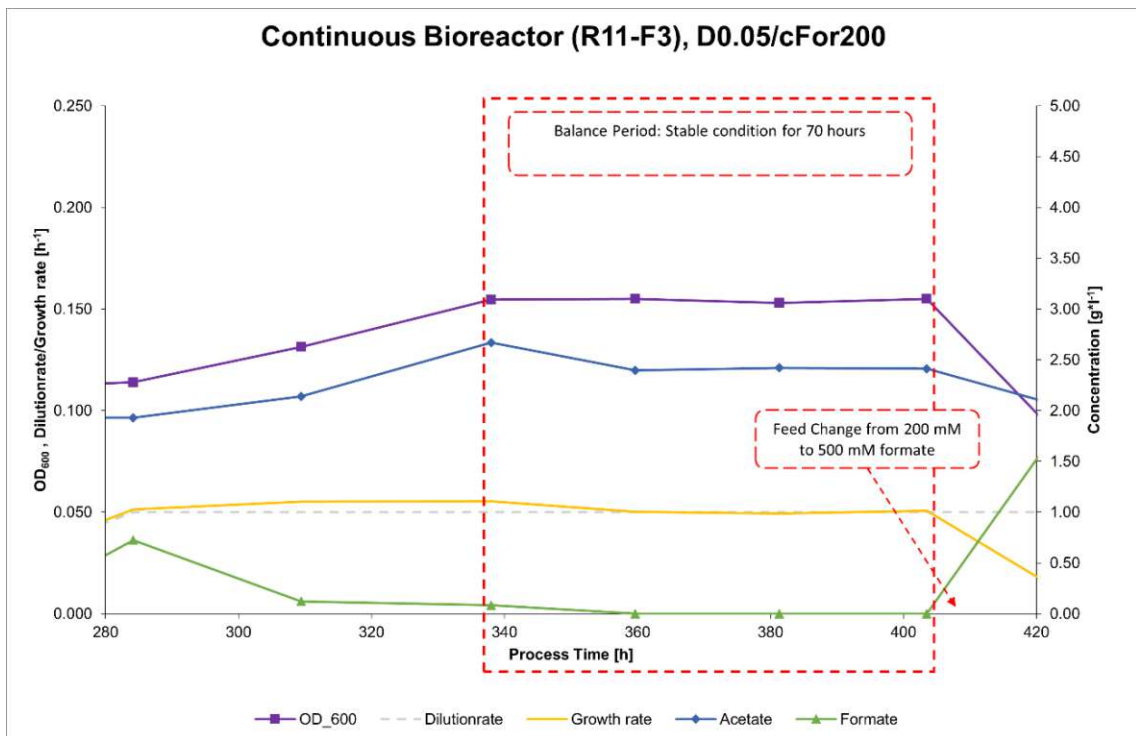
Figure 25: Continuous Bioreactor (R11-F3), D = 0.050 h^{-1}; c$_{For}$ = 200 mM

Figure 26: Continuous Bioreactor (R11-F4), D = 0.025 h^{-1}; c$_{For}$ = 300 mM
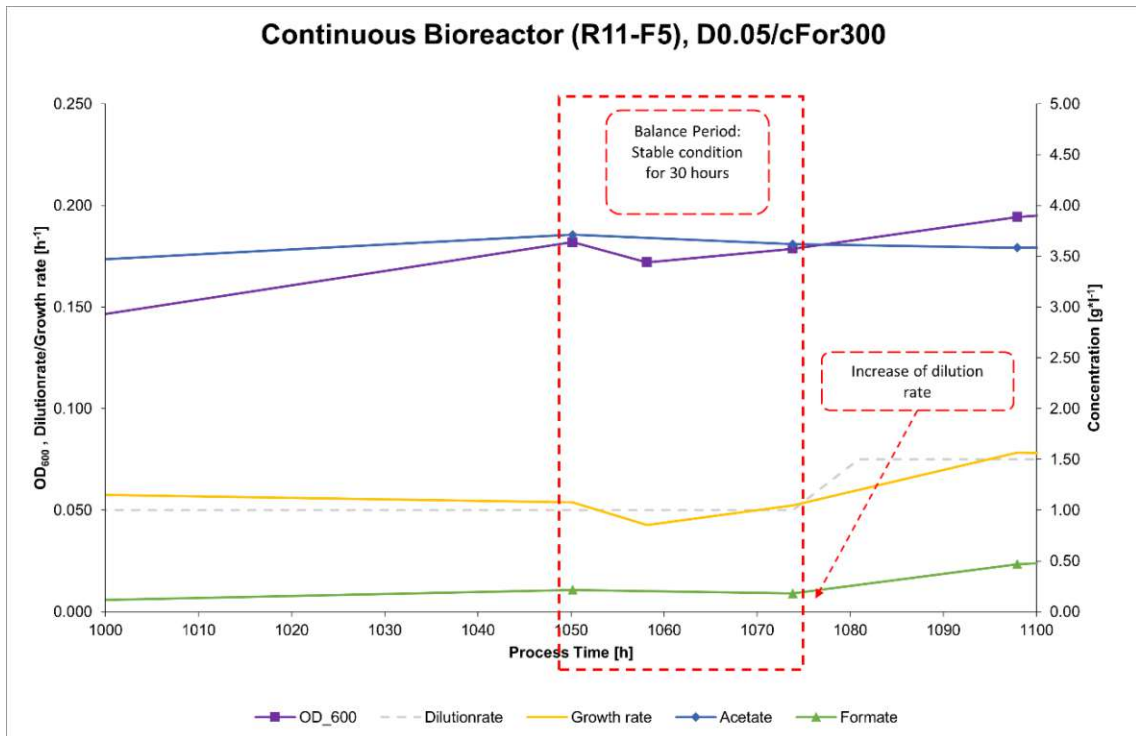
Figure 27: Continuous Bioreactor (R11-F5), D = 0.050 h^{-1}; c$_{For}$ = 300 mM
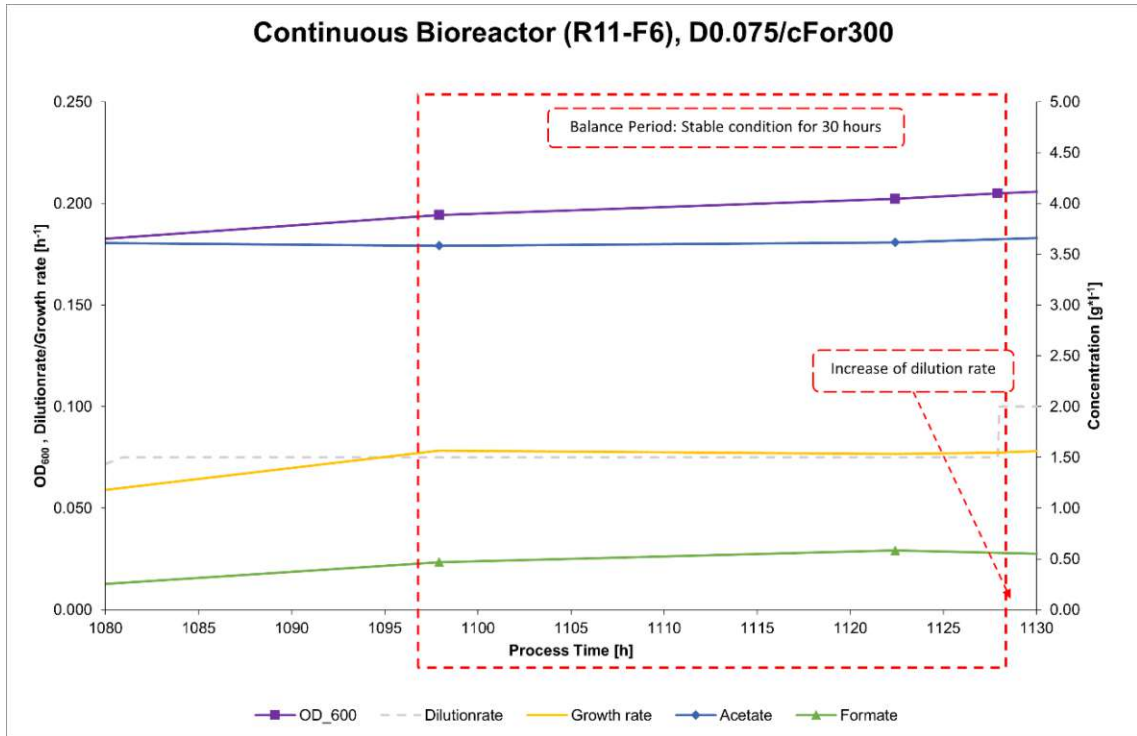
Figure 28: Continuous Bioreactor (R11-F6), D = 0.075 h^{-1}; c$_{For}$ = 300 mM
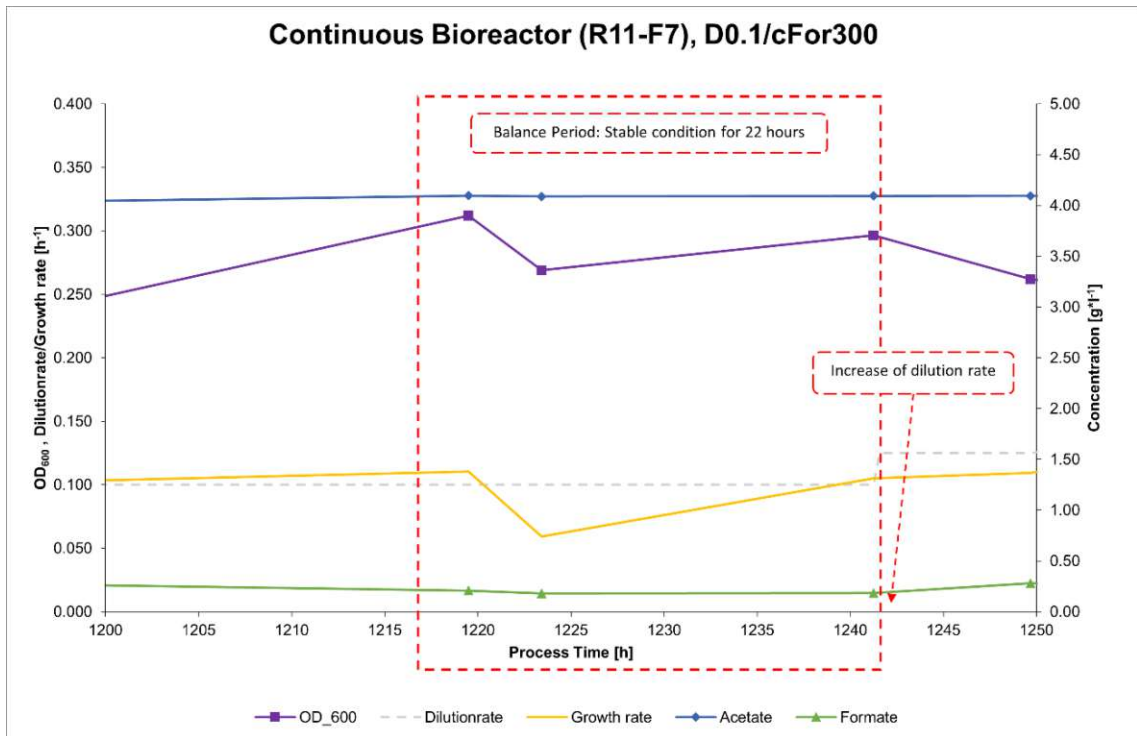
Figure 29: Continuous Bioreactor (R11-F7), D = 0.100 h^{-1}; c$_{For}$ = 300 mM
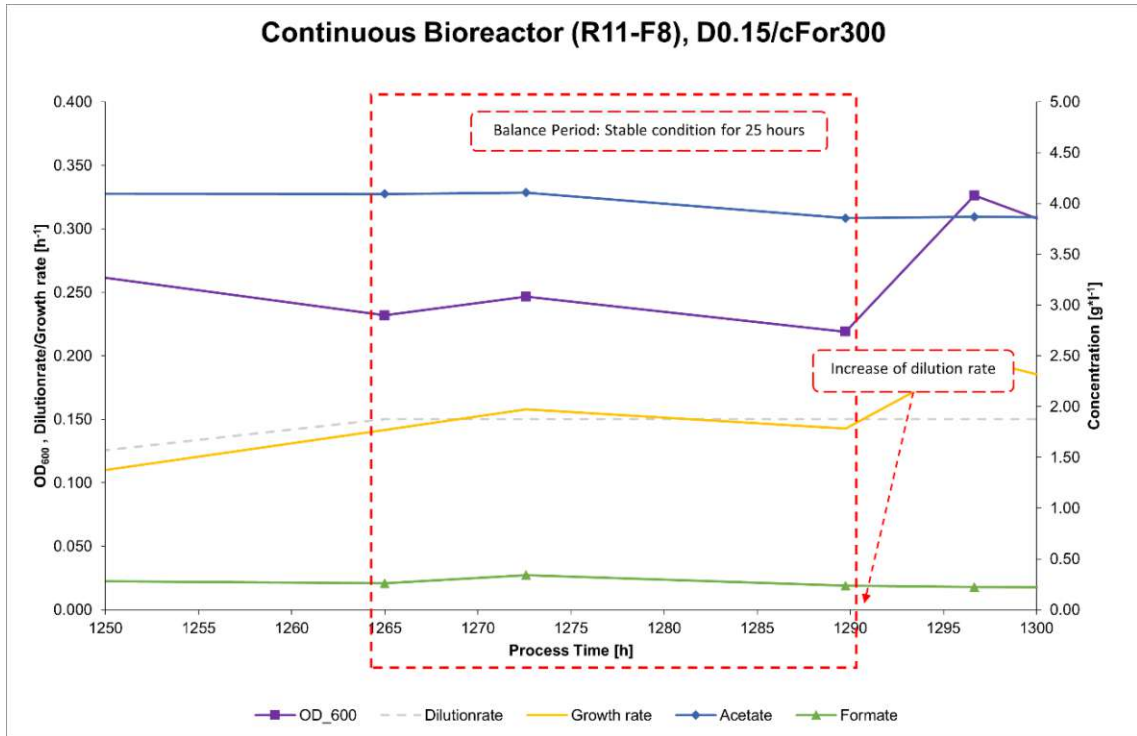
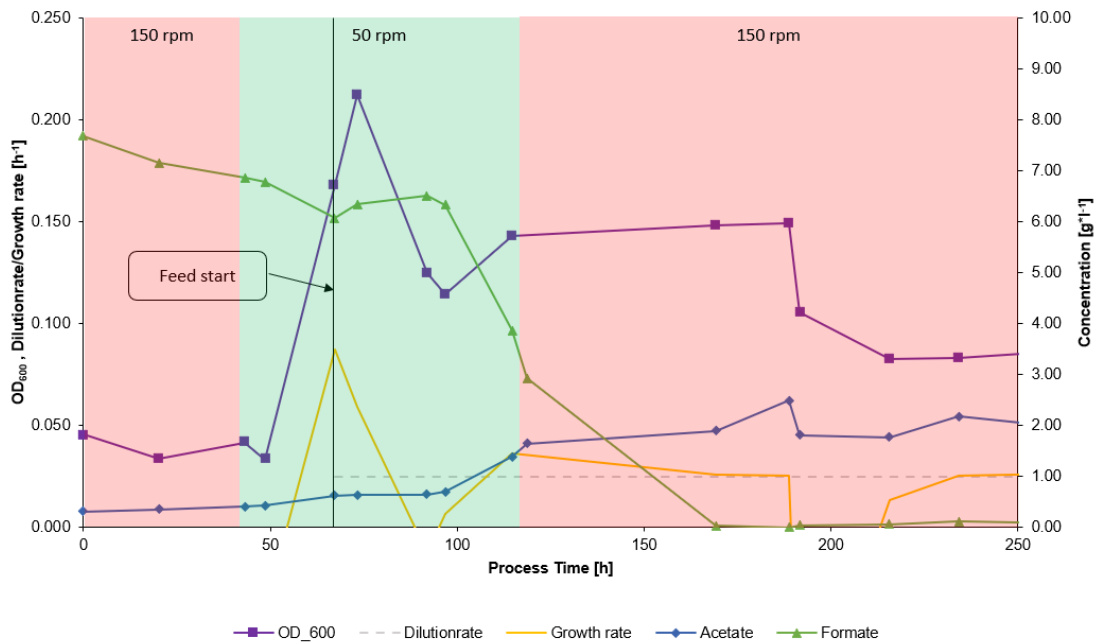Figure 30: Continuous Bioreactor (R11-F8), D = 0.150 h^{-1}; c_{For} = 300 mM

Figure 31: Start-up of Continuous Bioreactor (R8-F2), D = 0.025 h^{-1}; c_{For} = 200 mM
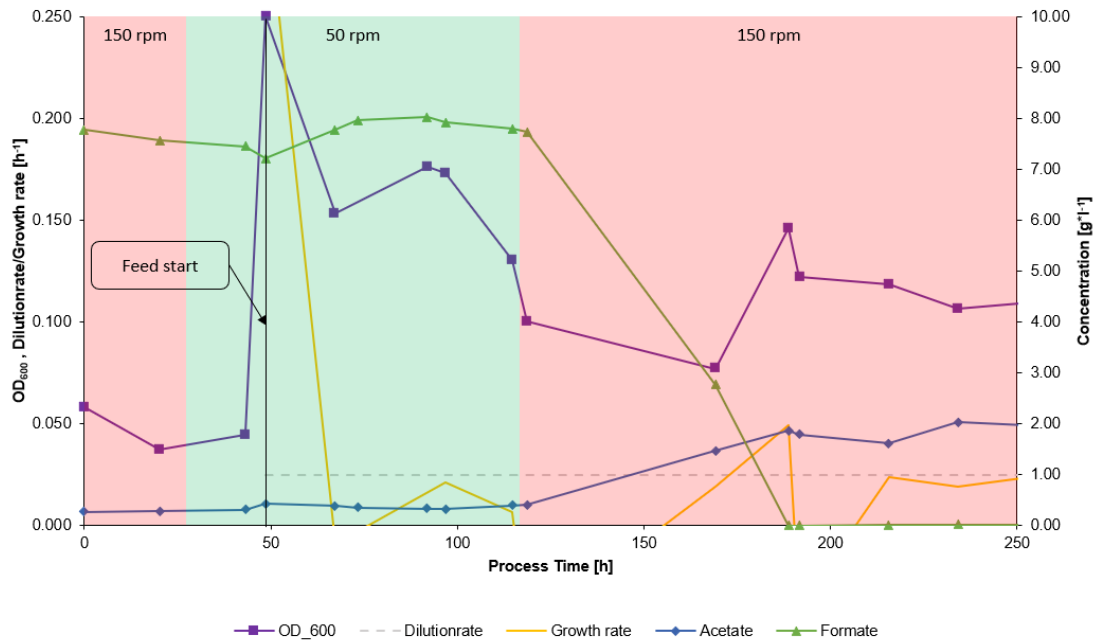
Figure 32: Start-up of Continuous Bioreactor (R11-F2), D = 0.025 h^{-1}; c$_{For}$ = 200 mM

Statutory declaration

„Hiermit erkläre ich, _____ *, an Eides statt, dass ich die vorliegende Masterarbeit selbstständig verfasst und keine anderen als die angegebenen Quellen und Hilfsmittel benutzt habe."*

_____

Ort, Datum, Unterschrift